REVIEWS OF

MODERN PHYSICS

VOLUME 42, NUMBER 2 APRIL 1970

Tunneling States of Defects in Solids*

V. NARAYANAMURTI† AND R. O. POHL

Laboratory of Atomic and Solid State Physics, Cornell University, Ithaca, New York 14850

The various optical, caloric, dielectric, elastic, and microwave investigations which have been used to study the tunneling states connected with the motion of atomic and molecular impurities in alkali halides are reviewed.

CONTENTS

I. TUNNELING STATES, A SPECIAL GROUP OF IMPURITY MODES

An atom or a molecule with several equilibrium orientations in its lattice site can perform a tunneling motion. The tunneling states of these ions represent a special group of impurity modes with a number of interesting properties:

(1) Their frequencies are small compared to the Debye frequency of the host, whose normal mode density of states is very low in this frequency region. These impurity modes can, therefore, often be considered separately from the motional states of the host, which makes their theoretical treatment particularly simple. In cases where the motion of the lattice has to be included, the Debye model can serve as a good approximation because of the low frequencies involved.

(2) Although the tunneling modes are relatively weakly coupled compared to the in-band impurity modes of higher frequency, they are still pronounced phonon resonant scatterers. Consequently they lend themselves to the study of phonon-defect interaction.

(3) Most tunneling states are electrically polarizable. Hence the defects behave like a gas of electric dipoles. This fact allows the study of the dielectric properties of a gas without the limiting influence of condensation at low temperatures.

(4) Finally, the tunneling states can be considered as the electric analogs to the magnetic spin states of defects and therefore allows one to do a variety of experiments previously restricted to the spin states.

Since the nature of these tunneling states was first established, they have been investigated extensively by a number of different methods. In this paper, we want to review this work and to point out how these impurity modes can be used as tools in the field of lattice dynamics, in particular for the study of phonon-defect interaction, and for a variety of dielectric investigations.

The outline of the article is as follows: Chapters II–IV contain a historical and theoretical introduction to the problem of tunneling and of tunneling states. Chapter V reviews the experimental and theoretical work which helped to establish the existence of tunneling states in solids. Chapter VI discusses three different topics which have been of particular interest to the authors. Information about the tunneling states is summarized in Fig. 37 and in VI.D, Table I.

* This work was mainly supported by the U.S. Atomic Energy Commission under Contract No. AT(30-1)-2391, Technical Report No. NYO-2391-98. Additional support was received from the Advanced Research Projects Agency through the use of space and technical facilities of the Materials Science Center at Cornell University, MSC Report No. 1220.

† Present address: Bell Telephone Laboratories, Murray Hill, N.J. 07974.

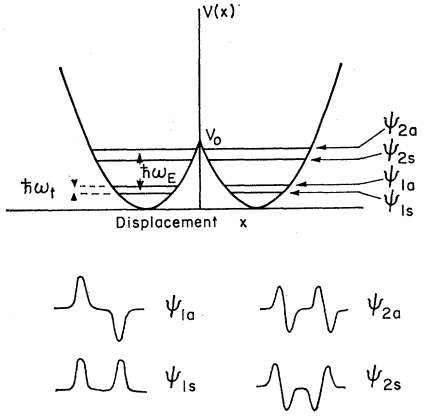

FIG. 1. Model potential of the one-dimensional, translational, double-well harmonic oscillator, top; and wavefunctions of the four lowest oscillatory states, bottom. $\hbar\omega_t$ is the tunnel splitting of the oscillatory groundstate. $\hbar\omega_E$ is the harmonic oscillator energy in the limit of large V_0. After Hund (Hu27).

Following common spectroscopic usage, we often give frequencies in wavenumbers. Quantities thus measured are labeled with a tilde ($\sim$). In the wavenumber measure "1 cm^{-1}" corresponds to a frequency $f=3\times10^{10}$ sec^{-1}, to an energy $W=1.24\times10^{-4}$ eV, and to a temperature $T=1.44°K$.

II. TUNNELING IN MOLECULES. HUND, THE AMMONIA INVERSION

When Hund (Hu27) applied the new quantum mechanics to the theory of molecular spectra, he formulated the following problem: The atoms in a polyatomic molecule can exist in configurations which are different but which, nevertheless, are energetically identical. A well-known example is the sugar molecule, which can exist in the form of two optical isomers. The one isomer turns the plane of polarization of a light beam to the right, and the other one turns it to the left. The two molecules are mirror images of each other, and hence the potential energies of both molecules are identical. At equilibrium, the two species are expected to exist in equal concentrations, yet right-turning sugar is known to remain so for very long periods of time without converting to the equilibrium mixture. Other examples are provided by living organisms: A man with his heart on the left side is energetically just as likely as his mirror image who has his heart on the right side. The fact that a man's heart is almost always on the left side means that over many thousand years and many generations the genetic information has not switched from left to right. In the classical picture these stabilities are easily explained: The energy barrier separating the two configurations is so high compared to k_BT that a flipover becomes very unlikely. Hund then asked whether such a high stability could also be explained with a quantum mechanical picture where the particle is described by a wave which is not confined to a potential well as strictly as a classical particle is. He studied this question for a particle subjected to a two-well harmonic potential, see Fig. 1, or specifically for the ammonia molecule NH_3, where the nitrogen has equilibrium positions above and below the plane formed by the three hydrogen atoms. The results of his investigation, which can now be found in many textbooks on quantum mechanics (see, e.g., Me61, Fe65), are briefly summarized. The oscillatory states occur in pairs; the separation between the pairs is approximately $\hbar\omega_E$, where ω_E is the harmonic-oscillator frequency for the single well. Each pair consists of a symmetric state of lower energy and an antisymmetric state of higher energy. The wave functions of the lowest two pairs of states are shown in Fig. 1. In each of these stationary states the particle is found with equal probability in either well. Hence, if the particle is consistently found in the same well, which for the example of the sugar molecule means that the sugar is observed to be, say, right-turning, then it is not in one of its stationary quantum states. Instead, the state is described as a linear combination of the symmetric and the antisymmetric stationary states. The resultant wave function is time dependent in the sense that it moves back and forth between the two wells with the angular frequency $\omega_t=\Delta E_t/\hbar$, where ΔE_t is the energy difference between the two stationary states. In contrast to the thermally activated process, this motion is temperature independent, and is called tunneling. It is worth emphasizing that the statement that the particle is tunneling between the different equilibrium positions is meaningful only if the particle is initially at least partially localized in one of the wells. A particle in a stationary state is not tunneling, although the process of observing it in such a state may cause a perturbation resulting in a tunneling motion.

For the double-well harmonic oscillator, the tunneling frequency ω_t between the lowest two states is

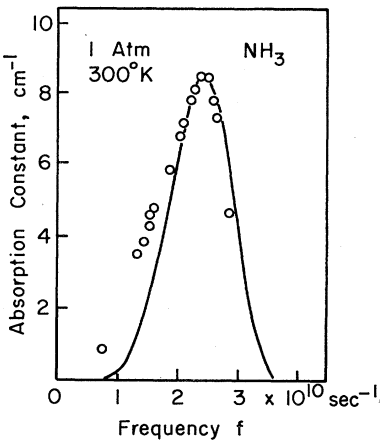

FIG. 2. Microwave absorption of gaseous ammonia. Absorption constant α defined by $I=I_0\exp(-\alpha x)$, where I and I_0 are transmitted and incident microwave intensities, respectively. Length of cell $x=40$ cm. After Cleeton and Williams (CW34).

given to a very good approximation by (Me61)

$$\omega_t = \Delta E_t/\hbar = 2\omega_E(2V_0/\hbar\omega_E\pi)^{1/2}\exp(-2V_0/\hbar\omega_E) \quad (1)$$

if the barrier height $V_0 > \hbar\omega_E$. Because of the exponential form in Eq. (1), ω_t depends critically on the ratio of barrier height to oscillator energy. Hund showed that for a typical $\hbar\omega_E = 10^{-1}$ eV (1000 cm^{-1} in the wave-number measure), the tunneling period varied between 10^{-9} sec and 10^9 year if $2V_0/\hbar\omega_E$ varied between 10 and 70. Consequently, a modest barrier height V_0 of several electron volt could produce an essentially infinitely stable molecule.

The existence of a finite tunnel splitting was first suggested by Dennison and Barker (Ba29) in their attempt to explain a fine structure of the order of a few inverse centimeters observed in the infrared absorption spectrum of gaseous NH_3. The first direct experimental observation of the tunneling transition, obtained by Cleeton and Williams (CW34) through microwave absorption experiments, is shown in Fig. 2. Maximum absorption occurs at $\nu_t = \omega_t/2\pi = 2.4\times 10^{10}$ sec^{-1} (0.8 cm^{-1}). For a detailed discussion of high-resolution measurements performed on the tunneling transitions of ammonia, which have proved beyond any doubt the correctness of Hund's prediction, we refer to the book by Townes and Schawlow (TS55).

It is of historical interest to mention that the work by Hund represents the first instance of the study of the wave-mechanical particle penetration of a barrier. It precedes the study of electronic tunneling out of metals and out of hydrogen (No27, Op28) and also precedes the celebrated explanation of radioactive decay (Ga28, GC28).

III. TUNNELING IN SOLIDS. THEORETICAL BACKGROUND

The question of tunneling of molecules in solids first arose when Pauling investigated how the rotational states of free molecules were modified when they crystallized into a lattice (Pa30). He approximated the crystal field by a cosine potential,

$$V = V_0(1-\cos 2\theta), \quad (2)$$

where θ is an angular coordinate for a rotation occuring

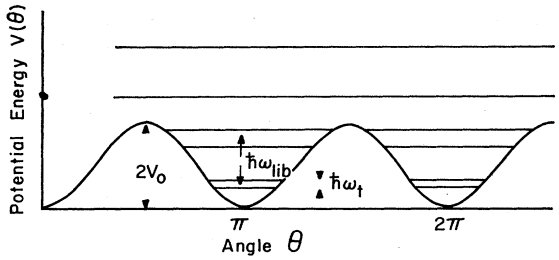

FIG. 3. The potential function $V = V_0(1-\cos 2\theta)$ used by Pauling (Pa30). Indicated are the tunnel split librational states near the bottom of the wells and the essentially free-rotor states at energies above the potential barrier. Schematic.

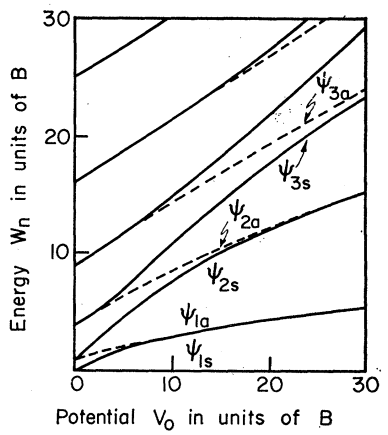

FIG. 4. Energy eigenvalues W_n in units of B, as a function of V_0/B, after Ta51.

in one plane. Such a potential has two minima as sketched in Fig. 3. The Schrödinger equation for this case is the Mathieu equation, and Fig. 4 shows its eigenvalues for the lowest states as a function of the potential parameter V_0 (Ta51). Energy W and V_0 are plotted in units of B, the rotational constant of the molecule, defined as

$$B = \hbar^2/2I, \qquad (\tilde{B} = \hbar/4\pi cI = B/hc), \quad (3)$$

where I is the rotational inertia of the molecule. Note that the energies of a free rotor are given by

$$W_J = BJ(J+1), \quad (4)$$

where J is the rotational quantum number. As V_0 increases, the free rotor states, particularly the ones with energies below the barrier height $2V_0$, are perturbed. These states are better described as states of angular oscillation, and in order to distinguish them from other oscillatory states, for instance, those of internal molecular vibration, they are called librational states. These librational states form pairs, and the energy splitting within each pair is the tunnel splitting. The states near the bottom of the potential wells are very similar in the models of Hund and Pauling, with the exception that the spacial coordinate is translational (x) in the one, and rotational (θ) in the other case. The difference between the two models becomes apparent only for states near and above the top of the barrier: In Hund's case, these states are oscillator states; in Pauling's case, they are rotor states.

Several investigators (St30, Fo35, Ni35, De36, Cu38, GPB54, KH66) have extended Pauling's calculation to three dimensions. We review only the work of Devonshire (De36), which has been particularly useful for the understanding of the tunneling states. He calculated the effect of a crystalline field of octahedral symmetry on the rotational states of a linear molecule. For this, he chose a potential of the form of the lowest-

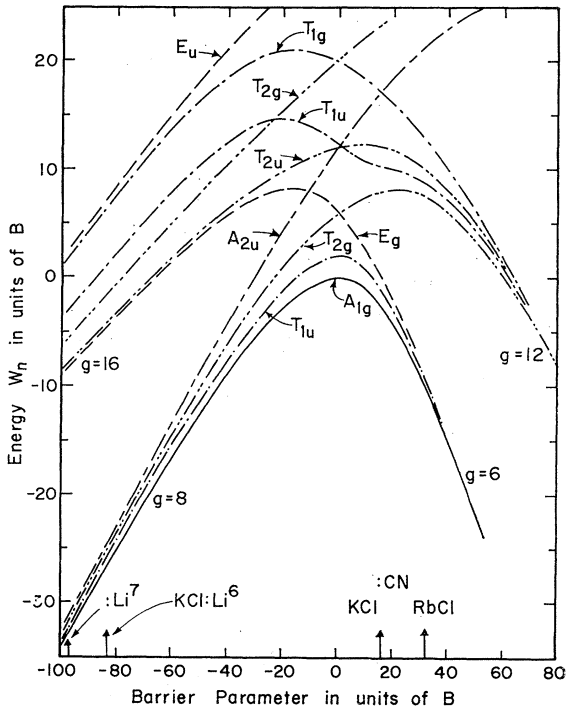

FIG. 5. Influence of the Devonshire potential on the lowest rotational states of a linear molecule of rotational constant B. Energy W_u and potential parameter K in units of B. With increasing barrier height the librational frequencies increase and the tunnel splittings decrease. Note how the states bunch up in groups for large $|K|$, i.e., in the limit of the tunnel split librational states. g is the total number of states in this limit. After De36 and Sa66. In the limit of large negative K, the librational ground state is split into four states of equal energy difference Δ; and for large positive K, the ground state splits into three states of energy difference 2Δ (A_{1g} to T_{1u}) and Δ (T_{1u} to E_g), respectively. These limits of large $|K|$ can also be computed starting from isolated pocket states, and allowing a certain overlap between adjacent states. The arrows indicate the barrier parameters determined experimentally for CN^- in KCl and RbCl, and for the two Li^+ isotopes in KCl, as described in Chapter V.

order surface harmonic:

$$V_{\mathrm{Dev}}=-2(4\pi/21)^{1/2}K[(7/12)^{1/2}Y_4^0 + (5/24)^{1/2}(Y_4^4+Y_4^{-4})], \quad (5)$$

$$V_{\mathrm{Dev}}(\theta,\phi)=-K\tfrac{1}{8}(3-30\cos^2\theta + 35\cos^4\theta+5\sin^4\theta\cos 4\phi), \quad (6)$$

where θ and ϕ are polar coordinates and K is the so-called potential parameter. The same potential also has played an important role in the crystal-field theory of paramagnetic electrons (Be29). For $K>0$, V_{Dev} has six minima in the directions

$$\theta=0 \text{ or } \tfrac{1}{2}\pi; \quad \text{and} \quad \theta=\pi,\ \phi=0,\ \pm\tfrac{1}{2}\pi, \text{ or } \pi, \quad (7)$$

which correspond to the six ⟨100⟩ directions in a cubic crystal. Potential maxima occur in the following directions:

$$\theta=\cos^{-1}[\pm(1/\sqrt{3})], \qquad \phi=\pm\tfrac{1}{4}\pi,\ \pm\tfrac{3}{4}\pi. \quad (8)$$

Such a potential may be used if the molecule has equilibrium orientations pointing along the ⟨100⟩ directions of a cubic crystal. For $K<0$, the maxima and minima are inverted, and this potential may be used if the molecule has equilibrium orientations along the eight ⟨111⟩ directions. For all K, V_{Dev} has saddle points in the twelve ⟨110⟩ directions, and the tunneling will occur via the ⟨110⟩ directions separating two neighboring wells. The potential difference between the bottom of the wells and the saddle points corresponds to the quantity $2V_0$ in Pauling's case, Fig. 3. This energy difference ΔV is

$$\Delta V=0.41K. \quad (9)$$

The eigenvalues of the Schrödinger equation for a molecule of rotational constant B in such a potential are shown in Fig. 5. They were computed by Devonshire (De36) and also recently by Sauer (Sa66). With increasing $|K|$, the energies in Fig. 5 change from those of the free rotor W_J [Eq. (4)] to those of a librator librating in six or eight wells, respectively. In the limit of large $|K|$, the low-lying librational states can also be calculated by starting from the wave functions describing the libration of the particle confined to one of the potential wells assumed to be purely harmonic. The tunnel splitting is then caused by the overlap of these localized wavefunctions (SSS65, Sh66b).

A direct extension of Hund's one-dimensional, double-well, translational oscillator to three dimensions and n wells was studied in detail by Baur and Salzman (BS66) and by Gomez, Bowen, and Krumhansl (GBK67). Gomez *et al.* considered elliptic potential wells, i.e., different harmonic-oscillator force constants for translations in x, y, and z, and also included the overlap of the wave functions (pocket states) in all n wells. Such a general case suffers from too many adjustable parameters, and so Gomez *et al.* focused their attention on the case of spherical potential wells for which significant overlap occurs only between nearest wells. For six or eight potential wells along the ⟨100⟩ or ⟨111⟩ crystallographic directions of a cubic crystal, respectively, the translational harmonic-oscillator states well below the potential barrier then turn out to be identical to those obtained with the Devonshire model (for $K>0$ and $K<0$, respectively), just as Hund's and Pauling's states are equal in this limit. For a quantitative comparison, the particle of mass m oscillating in n wells at the distance r_0 from the center of symmetry, has to be replaced by a quasi-molecule of rotational inertia mr_0^2 librating in these n wells.

Both the three-dimensional models of librational and of translational motion will be used in this paper.

IV. HISTORICAL INTRODUCTION TO THE PROBLEM OF ROTATIONAL MOTION AND OF TUNNELING IN SOLIDS

Since Pauling's paper (Pa30), several investigators have tried to detect the different stages of molecular

motion with a variety of techniques and with varying degrees of success. Most of the work has involved attempts to detect the change from libration to free rotation proposed by Pauling. Even though tunneling, which forms an integral part of Pauling's model, has been explicitly suspected in only a few instances, a brief review of some of these early experiments is made for the sake of completeness and historical interest.

The most thoroughly investigated molecular solid is hydrogen. In fact Pauling's theory was motivated by a calculation of the entropy of crystalline hydrogen by Giauque and Johnston (GJ28) and the measurements of Simon, Mendelsohn, and Ruhemann (SMR30). The motional states of solid hydrogen have since been studied by means of specific heat (HR54), infrared (GHAW60), Raman (BaW62, HSMcT69), and NMR (HR49, DM65) measurements. These measurements have shown that the barrier to rotation in hydrogen is very low and that the energy levels correspond very nearly to those known for the free molecule.

Besides hydrogen, several other molecular solids have been investigated. Most of the early experiments involved measurements of the specific heat or dielectric polarization (in the case of polar molecules) of pure molecular solids like the ammonium halides and hydrogen halides. The first suggestion that molecules in solids may possess a "limited degree of orientational freedom" was made by Debye (De29) in order to interpret the dielectric measurements on ice made by Errera (Er24). For early reviews of the specific heat and dielectric measurements the reader is referred to the papers by Eucken (Eu39, St61) and by Smyth (Sm36). More recently the specific heat of many pure molecular solids has been remeasured by Stephenson *et al.* (SLC52, SBS52, SRS55, SBS55). In every instance sharp discontinuities in the specific heat and dielectric constant were observed at a critical temperature T_c which varied from solid to solid. X-ray (KPH31, Si49, La49) and neutron-diffraction (LP53) studies have indicated crystal structure changes at T_c. This behavior can be qualitatively explained on the basis of Pauling's model as a change from libration to free rotation or, alternatively, on the basis of Frenkel's model (Fr46, La37), as an order–disorder transition.

Recent measurement of proton nuclear magnetic resonance (GP50, GPB54a, An50, RS61, CBG63, CG64), inelastic neutron scattering (RTH60, Pa62, BBSP63, VDVR64, YO63), and particularly infrared absorption (WH50, SH62, He58, Ew62, Ew64), however, have unequivocally shown that for all molecular solids, with the sole exception of solid hydrogen, the Frenkel picture is the correct one and that the barrier to rotation is extremely high; the primary motion of molecules in these solids is librational together with a thermally activated reorientation process at elevated temperatures leading to a disordered state. In none of the above examples has tunneling been observed. This is consistent with the high barrier to rotation since the tunneling frequency depends exponentially on the barrier height.

It is not too surprising that Pauling's model has not been more successful for molecular solids since a stationary potential, as used in Eq. (2), should not be expected to describe a cooperative phenomenon as, for instance, the onset of rotation of all the molecules in the molecular crystal.

In addition to the work on pure molecular solids cited above, in recent years several experiments have been performed on molecules trapped in inert-gas matrices and in β-quinol clathrate. Most of these studies have been made using the techniques of infrared spectroscopy and, in the case of magnetic molecules, by means of ESR and magnetic susceptibility. Among the molecules which have been studied are HCl (SMKW62, BF66), H_2O (RM62, Ro63), CH_4 (CSH63), NH_2 (RM59, Je60), and NH_3 (MHD61) in inert-gas matrices; O_2 (MOV57), KO (Me61a, BMR65), and N_2 (MS59) in the clathrate; and the oxygen atom in silicon and germanium (HA60). These measurements, which were interpreted with Pauling's model, have shown that the barrier to rotation is low for many molecules in these materials and that in some of the above cases the spectra can be qualitatively described on the basis of models of hindered rotation and possibly tunneling.

A detailed study and understanding of the tunneling states evolved with the study of atoms and molecules incorporated substitutionally in alkali halide crystals. Among the early studies the work by Känzig (Ka62) on the O_2^- ion in alkali halides deserves special mention. At low temperatures the ESR spectrum of this ion consists of six lines, each line corresponding to one of the six $\langle 110 \rangle$ axes in the crystal. Application of uniaxial stress lifts the sixfold orientational degeneracy, and the population changes are observed by monitoring the intensities of the paramagnetic resonance lines. Känzig found that above 4.2°K the measured populations of the different orientations agreed with Boltzmann statistics and the assumption that the strain energies ΔU are proportional to the applied stress σ. The coefficients of proportionality (the so-called components of the elastic dipole moment tensor) were found to be of the order of 5×10^{-24} cm^3. In addition to the static alignment studies, Känzig studied the kinetics of the reorientation process and found that below 4.2°K the reorientation times τ increased as T^{-1}. This temperature dependence indicated that the molecular reorientation was accompanied by the simultaneous emission or absorption of a single phonon. Sussman (Su64) proposed that the molecular reorientation of the O_2^- took place via a tunneling process. However, if the different molecular orientations are made inequivalent due to the presence of an external or random internal stress, then the tunneling can only occur by means of simultaneous emission or absorption of a phonon in order to conserve energy. Silsbee (Si67) has given a particularly

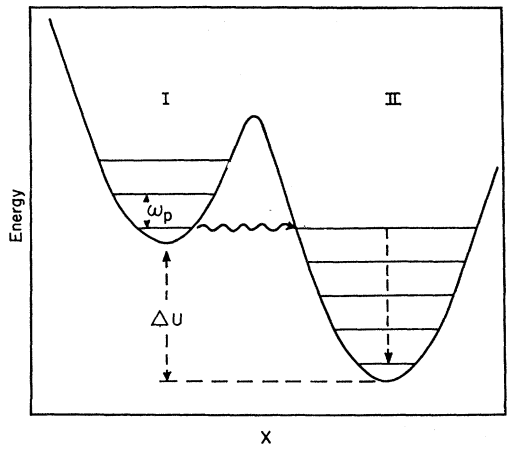

FIG. 6. Configuration coordinate model for the O_2^- reorientation, after Silsbee (Si67). The potential shown in the figure represents the energy of O_2^- plus lattice when the molecule is localized in either of the two wells, as a function of host ion positions. The localization energy ΔU, which is much larger than the tunneling matrix element (times $\hbar$), may be varied by stressing the crystal. The molecule can make a transition from one orientation to the other by tunneling through the barrier with simultaneous emission or absorption of a phonon of energy $\Delta U = n\hbar\omega_p$ in a n-phonon process.

lucid physical description of this process in terms of a configuration coordinate model as shown in Fig. 6. Sussman showed that if k_BT is greater than the energy difference between the wells, then τ for such a one-phonon induced tunneling process should be proportional to $\sigma^{-2}T^{-1}$. For small values of the stress σ, Känzig found τ to be independent of σ. This departure from theory can be explained by assuming (Su64) the presence of internal stresses of the order of magnitude of 10^8 dyn/cm^2. The calculations of Sussman have been extended to include multiphonon processes by Pirc, Zeks, and Gosar (PZG66). Recent experiments by Silsbee (Si67) and by Pfister (Pf69), involving a change in the oxygen isotopic mass, confirmed that tunneling is important in the molecular reorientation process. By comparing experiment with theory Silsbee found that the tunnel splitting is of the order of 10^{-6} cm^{-1} (wavenumber measure). Because of this small value of the tunnel splitting and the large stabilization of the O_2^- molecules into a particular orientation by the internal strains, the effects of mixing of other orientations is experimentally unobservable except for the reorientation process itself.

We would also like to mention the possibility of the tunneling of Jahn–Teller ions between several equivalent lattice distortions (dynamic Jahn–Teller effect). The evidence for such dynamical effects consists primarily in the observation of motional averaging of the ESR spectrum for several Jahn–Teller systems (St67, BKW69). Chase (Ch69) has suggested that the tunneling levels themselves have been detected for the first time optically in the case of Eu^{2+} in CaF_2.

Finally we would like to mention shallow donors in silicon and germanium, since their electronic states (Ko57) resemble the motional states of tunneling ions in many of their properties. From symmetry considerations, the ground state, which should be sixfold degenerate in the case of silicon (fourfold degenerate in the case of Ge), because of the multivalley nature of the conduction band in these materials, splits into a singlet, doublet, and a triplet in Si, and into a singlet and a triplet in Ge. This splitting is called "valley–orbit splitting" or "chemical shift." The effect of uniaxial stress on the donor energy levels has been calculated by Price (Pr56) and Kohn (Ko57); its effect on the wave functions has been calculated by Fritzche (Fr62). The stress destroys the equivalence of the different conduction minima, splits the triplet state into a singlet and a doublet, and admixes the excited states to the ground state.

Wilson and Feher (WF63) have measured the ESR spectrum of P, As, and Sb doped Si under the influence of shearing strains of the order of 10^{-3}. From these measurements they found values of the order of 0.015 eV for the valley–orbit splitting. They have also measured the spin–lattice relaxation and found it to be proportional to $H^{-4}T^{-1}$, indicating a one-phonon process. Hasagawa (Ha60) and Roth (Ro60) have calculated the magnitude of the one-phonon relaxation by means of a simple theory involving the modulation of the valley–orbit splitting by the strain field of the lattice vibrations. Using the static strain coupling coefficients found from their ESR measurements, Wilson and Feher found excellent quantitative agreement with the model of Hasegawa and Roth. Similar measurements on the ESR spectra of donors in Ge have recently been reported by Pontinen and Sanders (PS60). Chemical shift in Ge has been determined directly from infrared absorption measurements by Reuszer and Fisher (RF64), who found the splitting to be 0.32 meV for Sb, 2.83 meV for P, and 4.23 meV for As in Ge.

Goff and Pearlman (GP61) found strong phonon scattering from shallow donors in Ge. Their thermal conductivity measurements have been extended by Bird and Pearlman (BP68). The effect on the thermal conductivity was first calculated by Keyes (Ke61). He considered an interaction arising from a static strain field which gives rise to an ω^4 dependence of the scattering. An additional frequency dependence arises when the phonon wavelength is less than the mean radius r_0 of the localized state, causing the average strain and hence the interaction to approach zero. Griffin and Carruthers (GC63) have argued that Keyes' static calculation is inappropriate when the phonon frequency is comparable to the valley–orbit splitting as is the case in the thermal conductivity measurements. They considered the dynamic response of the electron and treated the scattering by analogy with the well-known resonance fluorescence scattering of light by atoms. The results for Sb in Ge are shown in Fig. 7 as an example of the fit obtained. The value of the valley–orbit splitting

for Sb agrees with the earlier measurement. It is important to point out, however, that the thermal conductivity for As and P doped Ge does not show a resonance scattering; this is not well understood.

V. THE DETECTION OF TUNNELING STATES OF DEFECTS IN SOLIDS

This chapter reviews the investigations which established the existence and the nature of the tunneling states connected with atomic motions in solids.

A. The CN^- Ion. Devonshire Model

The first direct evidence for the existence of tunneling states of defects in solids was found in thermal conductivity measurements on KCl crystals containing KCN in small concentrations, see Fig. 8 (Se65). In the doped crystals the low-temperature conductivity was drastically reduced. Distinct indentations in the curves were noticed around 0.5 and 5°K, which indicated that the phonons carrying the major part of the heat at these temperatures were more strongly scattered than those carrying the heat above and below. These observations raised two questions: First, what is the nature of the centers causing this selective phonon scattering? Second, what can be learned about the phonon scattering cross sections from these thermal conductivity measurements? In this chapter, we shall

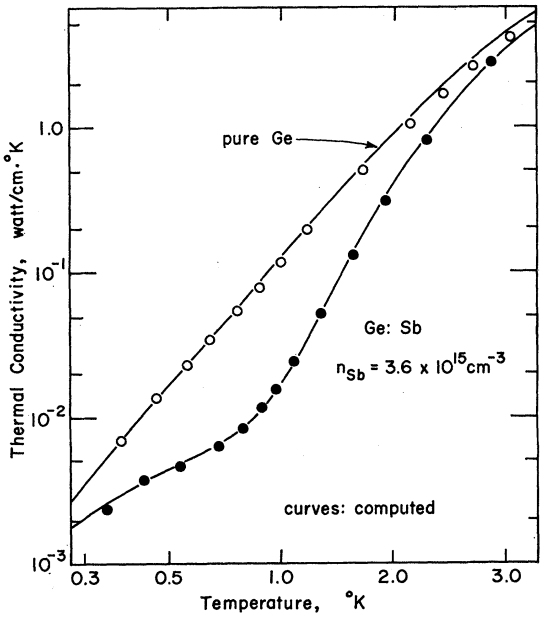

FIG. 7. Ge:Sb. Upper curve, pure Ge; lower curve, Ge containing 3.6×10^{15} cm^{-3} uncompensated Sb. Solid curves were computed using the Debye model of thermal conductivity (see VI.A). The conductivity of the doped crystal was computed with the phonon-defect scattering rate suggested by Griffin and Carruthers (GC63) using the shear deformation potential constant $E_u=16$ eV, the valley–orbit splitting $4\Delta_c=3.2\times10^{-4}$ eV, and the cutoff radius $r_0=44$ Å; all three quantities as determined by other experiments. After Bird and Pearlman (BP68).

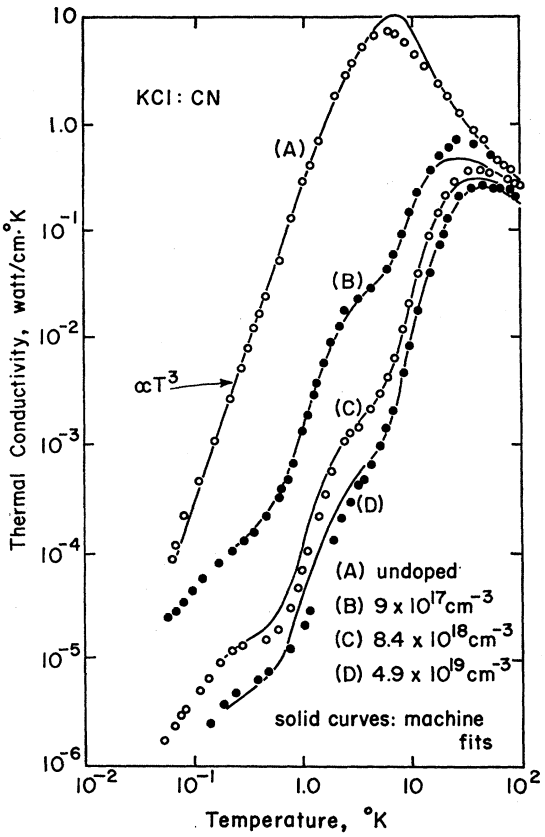

FIG. 8. Thermal conductivity of KCl:CN, after Se65 and SN66, extended to $T=0.05$°K by Harrison and Peressini (unpublished data). The solid curves which should be ignored in Chapter V were computed as discussed in VI.A.

study the first question, using thermal conductivity measurements merely as qualitative indicators for the existence of selectively scattering defects, and shall leave the question of the phonon-defect interaction to Chapter VI.

The selective phonon scattering suggests the existence of discrete states which are coupled strongly to the phonons and hence scatter them resonantly. An understanding of these states was obtained from a study of the near-infrared stretching vibration of the CN^- ion and from specific-heat measurements. We shall review this work in the following (Na64, SN66). The infrared absorption of KCl:CN at 300°K is shown in Fig. 9. Instead of a narrow line, the spectrum is a broad band with a characteristic double hump. Its shape is independent of concentration and unaltered after a slow anneal or a rapid quench from temperatures close to the melting point of the crystal. The identical shape is observed with the overtone vibration at 2.5 μ ($\Delta n=+2$), which demonstrates that the absorption is caused by the simultaneous excitation of the stretching vibration and some other states and not by, say, CN^- ions in a variety of surroundings. The nature of these states becomes apparent by comparison with the absorption

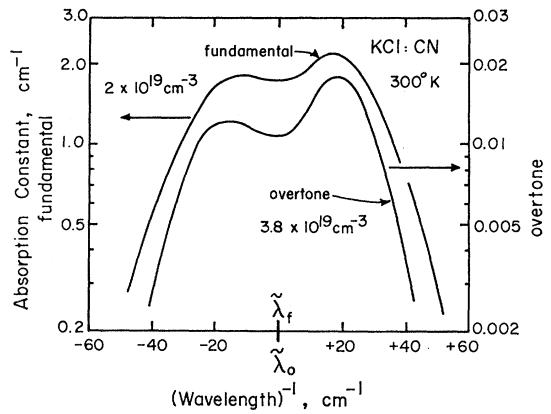

FIG. 9. Absorption by the stretching vibration of CN^- dissolved in KCl, at 300°K. Fundamental ($\Delta n=+1$) and overtone vibration ($\Delta n=+2$). Note that the shapes of both curves are almost identical. If the breadth of the fundamental absorption were caused by CN^- in a number of different surroundings, the overtone absorption would be twice as wide as the fundamental (SN66) $\tilde{\lambda}_f=2088$ cm^{-1}, $\tilde{\lambda}_0=4144$ cm^{-1}.

of a molecule (HCl) which is in the *gas* phase (Bu13) (see Fig. 10, in which the shape of the absorption band is very similar to that of the CN^- ion in solid solution). The origin of the band in the case of the gaseous molecule is well known. It is caused by an excitation of a stretching vibration ($\Delta n=+1$) and a simultaneous excitation or de-excitation of a rotational state ($\Delta J=\pm 1$). The different transitions are not resolved in Fig. 10, but the envelope, calculated from the selection rules of transition and the thermal population of the higher rotational states, agrees well with the observed band shape. The similarity of the molecular spectra in the gas phase and in the solid solution suggests that the molecule in the solid is also freely rotating. This picture was confirmed by a study of the temperature dependence of the CN^- spectrum. With decreasing temperature, the two humps move closer together. For a free molecule, the separation of the

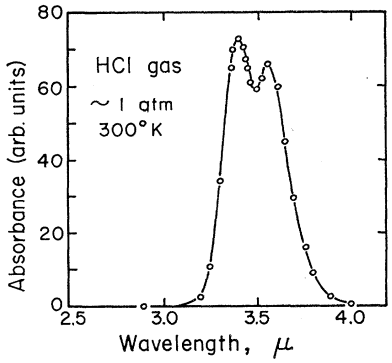

FIG. 10. Rotation–vibration spectrum of gaseous HCl, after Burmeister (Bu13). The double hump is characteristic of a diatomic molecule, for which the Q branch is forbidden. At higher resolution, the HCl spectrum splits into many narrow lines which are separated by 0.025 μ.

humps goes as the square root of T:

$$\Delta\tilde{\nu}_{PR}^{\max}=(8\tilde{B}k_BT/hc)^{1/2}. \tag{10}$$

This temperature dependence is indeed observed, see Fig. 11. In Eq. (10), the rotational constant $\tilde{B}$ [Eq. (3)] is the only unknown quantity and can be determined from the experiment:

$$\tilde{B}=1.25\text{ cm}^{-1}\pm 20\%\ (CN^-\text{ in KCl}), \tag{11}$$

and from this the internuclear distance

$$r_{C-N}=1.4\times 10^{-8}\text{ cm}\pm 10\%, \tag{12}$$

very close to the distance estimated on the basis of the ionic radii, $r=1.47\times 10^{-8}$ cm.

These observations lead to the remarkable conclusion that the CN^- ion in the KCl crystal behaves like a freely rotating molecule, at least above 60°K. Below this temperature, the spectrum changes drastically, as shown in Fig. 12. Between the two maxima observed

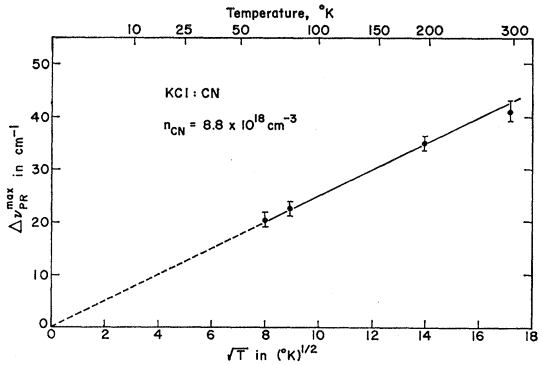

FIG. 11. Separation $\Delta\tilde{\nu}_{PR}^{\max}$ of the two maxima observed in Fig. 9 as function of temperature. $n_{CN}=8.8\times 10^{18}$ cm^{-3} (SN66).

at high temperatures, a narrow absorption band rises rapidly. Near 10°K, a satellite both at higher and lower energy is observed; the low-energy satellite disappears as the temperature is lowered even further, whereas the high-energy satellite (at $\Delta\tilde{\nu}=12$ cm^{-1}) grows in intensity. Again, the fundamental and the overtone absorption spectra are identical.

Below 60°K, the crystal field becomes noticeable. A qualitative understanding was achieved by approximating the cavity potential with Pauling's cosine function, Eq. (2). Below 10°K, only the librational states are populated. The selection rule for infrared absorption is that for two coupled oscillators (internal vibration, quantum number n, and libration, quantum number n_{lib}) (HD56):

$$\Delta n=+1,\ \Delta n_{\text{lib}}=0,\pm 1,\pm 2. \tag{13}$$

The transition probability decreases with increasing $|\Delta n_{\text{lib}}|$. In Eq. (13), the tunnel splitting of the librational states is ignored for simplicity. Note that in the harmonic approximation, Δn_{lib} is strictly zero.

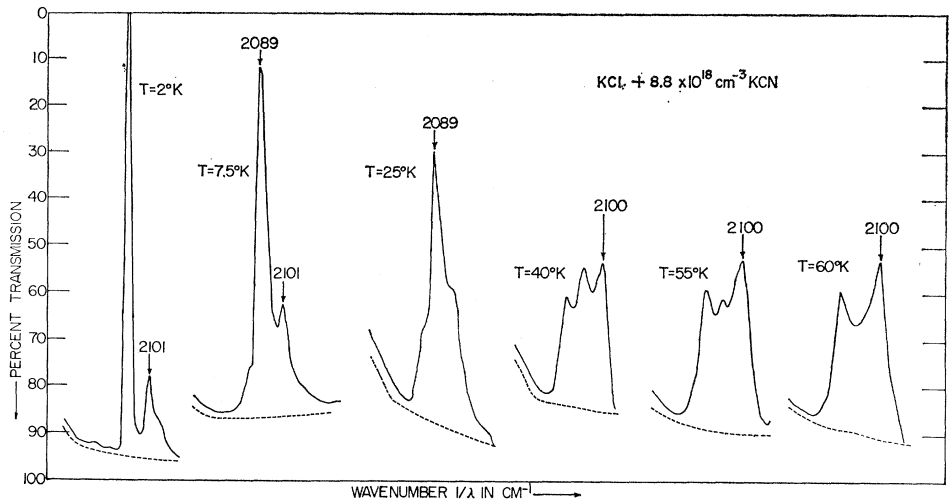

FIG. 12. Transmission spectra of KCl:CN in the region of the CN^- fundamental stretching vibration, at six different temperatures. $n_{CN}=8.8\times10^{18}$ cm^{-3}, sample thickness $t=0.5$ cm. Almost identical spectra were obtained in the overtone region (SN66).

The strong transition at 2089 cm^{-1} corresponds to $\Delta n_{lib}=0$, the weak sum satellite to $\Delta n_{lib}=+1$, and the weak difference satellite to $\Delta n_{lib}=-1$. The librational frequency is $\tilde{\nu}_{lib}=12$ cm^{-1}, and therefore the difference satellite vanishes below 10°K. With this librational energy, and with $\tilde{B}$ as determined at high temperatures, the solutions to Mathieu's equation, Fig. 4, can be used to determine the barrier height $2\tilde{V}_0=24$ cm^{-1}, corresponding to 35°K. This barrier agrees well with the observation that the influence of the potential becomes unnoticeable for $T>60$°K. With $2\tilde{V}_0$ known, the tunnel splitting of the librational ground state can be estimated. According to Fig. 4, it is expected to be 0.5 cm^{-1}. The strong transition $\Delta n=+1$, $\Delta n_{lib}=0$ (at 2089 cm^{-1}) should actually consist of two lines: one transition originating at $n=0$; ψ_{1s}, leading to $n=1$, ψ_{1a}, and the other at $n=0$, ψ_{1a}, leading to $n=1$, ψ_{1s}. These two transitions differ in energy by 2×0.5 cm$^{-1}=1$ cm^{-1}, an amount within the instrumental resolution of 0.6 cm^{-1}. Yet, only one line was observed. One can think of a number of reasons: (a) The interpretation of the librational satellites is wrong, and tunneling does not occur: (b) The molecule is indeed librating as described above, but Pauling's one-dimensional model is too crude, and the tunnel splitting of the three-dimensional librator is far smaller: (c) The tunnel splitting is indeed of the predicted magnitude, but somehow the tunneling levels are broadened and can therefore not be resolved. This would be possible since the half-width of the 2089-cm^{-1} band is about 2.5 cm^{-1}.

Next it shall be shown that even in the refined three-dimensional calculation a tunnel splitting of order 1 cm^{-1} is obtained (Na64, SN66). KCl is a cubic crystal, and hence Devonshire's calculations can be used if the equilibrium orientations of the CN^- molecule are known. They were obtained from a study of the stress-induced dichroism of the CN^- stretching vibration at low temperatures. The results, Fig. 13, show the potential minima point along the ⟨100⟩ directions: For stress $\sigma \parallel [100]$, maximum dichroism is observed; for $\sigma \parallel [111]$, it is smallest. Actually, for a ⟨100⟩ defect $\sigma \parallel [111]$ should produce zero dichroism. This discrepancy is ignored at this point, but will be taken up again in Chapter V.B. For a ⟨100⟩ defect, Devonshire's potential parameter K is positive. Electric dipole selection rules favor the transition $T_{1u}(J=1)$ to $T_{2g}(J=2)$ for the sum satellite, i.e., $\tilde{W}(T_{2g})-\tilde{W}(T_{1u})=12$ cm$^{-1}=9.6\tilde{B}$. As can be seen from Fig. 5, this requires a potential parameter $\tilde{K}=16\tilde{B}$, or $\tilde{K}=20$ cm^{-1}, see arrow in Fig. 5. The tunneling states consist of three partly degenerate levels; the splitting between the lowest (A_{1g}) and the first excited state (T_{1u}) is 1.4 cm^{-1}, and the splitting between T_{1u} and the next higher state (E_g) is 1.0 cm^{-1}. Hence Devonshire's model predicts an even larger tunnel splitting than Pauling's model did! Since the infrared spectrum fails to reveal a fine structure that might be ascribed to this splitting, but since conceivably the individual states are broadened to the point that the individual transitions cannot be resolved, a different experimental method which is less sensitive to a level broadening, such as specific heat, is used for the detection of the tunneling states. The results (SN66, PPHN69) are shown in Fig. 14: A large specific-heat anomaly is observed in crystals of KCl:CN. The total entropy ΔS is proportional to the chemically determined CN^- concentration n_{CN}:

$$\Delta S = n_{CN} k_B \ln 6, \tag{14}$$

the scaling factor is Boltzmann's constant k_B times ln 6, as is predicted if a total of six states are thermally populated. This number agrees with the six states predicted by the Devonshire model with $K>0$, i.e., with a ⟨100⟩ defect. The dashed curves are best fits using the Devonshire potential, for splittings of 1.15

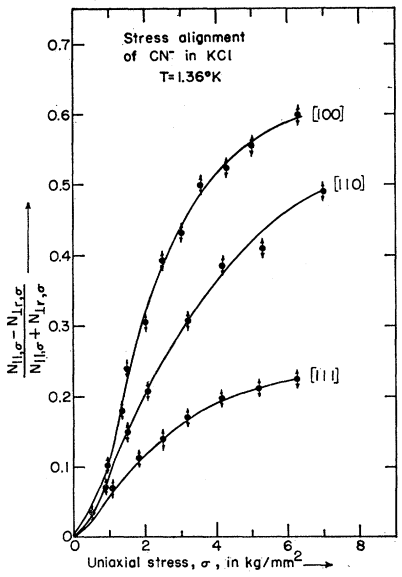

FIG. 13. Alignment of the CN^- ions as a function of uniaxial stress in KCl. $T=1.36°K$. For $[1\bar{1}0]$ stress the light was propagating in the $[1\bar{1}0]$ direction (SN66).

cm^{-1} ($A_{1g}-T_{1u}$) and 0.85 cm^{-1} ($T_{1u}-E_g$). These values are within 15% of the values predicted on the basis of the infrared data. The very good agreement between experiment and theory is taken as evidence for the correctness of the Devonshire model. This means in particular that the lowest six states are indeed tunneling states. The magnitude of the tunnel splitting is surprisingly large: 1.15 cm^{-1} (between A_{1g} and T_{1u}) is about one-half the energy of the first rotational state of the free CN^- ion, which is $\tilde{W}_1=2\tilde{B}=2.5$ cm^{-1} [Eq. (4)].

In the KBr and KI host lattices, phonon resonant scattering is similar to that in KCl. Also, the infrared data are very similar to those obtained in KCl, and hence the motional states are very similar. Nevertheless, there are a few differences, in particular at higher temperatures, for which we refer to the original paper (SN66). The rapid reorientation of the CN^- ions in the potassium hosts was also demonstrated by Sack and co-workers (SM65) through measurements of the ac dielectric constant. Figure 15 shows the excess dielectric constant $\Delta\kappa$ observed in KCl:CN. In the temperature range measured, $\Delta\kappa$ varies as T^{-1}. At lower temperatures, $\Delta\kappa$ saturates, and this saturation has been shown to result from the thermal depopulation of the excited tunneling states, at least at low concentrations. The tunnel splitting derived from the measurements is of the order of 1 cm^{-1} (BS66a) in agreement with the values obtained from the other experiments.

In RbCl:CN, the infrared spectrum was similar to that of KCl:CN, with a librational satellite 19 cm^{-1} away from the central line at low temperatures (SN66). Devonshire's model thus predicts a larger potential barrier and hence smaller tunnel splittings, $A_{1g}-T_{1u}$: 0.49 cm^{-1}, $T_{1u}-E_g$: 0.25 cm^{-1}, roughly one-half of the splittings found in the potassium hosts. Thermal conductivity measurements showed strong resonance scattering (HPP68), see Fig. 16, occurring at about one-half the temperature at which it occurred in the potassium hosts, Fig. 8. This scaling with the tunnel splitting suggests that the resonance scattering is caused by an interaction with the CN^- tunneling states. The studies of the RbCl:CN tunneling states using measurements of specific heat, paraelectric resonance, and electric field induced dichroism of the infrared stretching vibration will be reviewed in V.B.

In NaCl and NaBr hosts, finally, the infrared CN^- spectrum is completely different (SN66). A single, relatively narrow band, with a half-width $\tilde{H}=20$ cm^{-1} at 300°K, narrows as T^2 without showing any evidence of librational satellites. From the complete absence of a stress induced infrared dichroism between 1.36°K and 4.2°K over time periods as long as 10^3 sec, the barrier to rotation is estimated to be greater than 100 cm^{-1} [assuming a thermally activated reorientation process and a librational (attempt) frequency of 10^{12} sec^{-1}]. For a Devonshire potential with $\tilde{K}>80\tilde{B}$, the tunnel splitting is estimated to be $\ll 10^{-1}$ cm^{-1}.

That the splitting must be small was also indicated

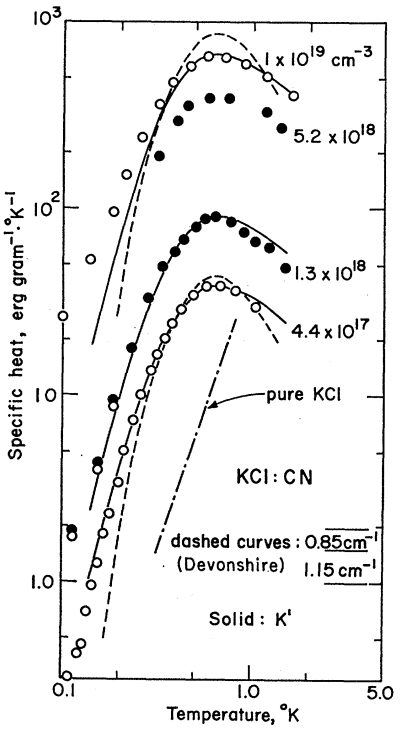

FIG. 14. Excess specific heat measured on crystals containing CN^- ions. Curves are computed Schottky specific-heat anomalies. The dashed curves are best fits using the Devonshire model, with the tunnel splitting as indicated in the figure. The solid curves are specific-heat anomalies computed using a tetragonally distorted Devonshire potential which will be discussed in V.B. The pure KCl specific heat, shown for comparison, is $C_{v,KCl}=46$ erg $gram^{-1}\cdot°K^{-4}T^3$ (SN66, PPHN70).

by dielectric measurements and by thermal conductivity, Fig. 17, which showed no sign of resonance scattering at low temperatures. The high-temperature resonant scattering is probably caused by a lattice resonant mode, or by rotational states close to or above the potential barrier (HPP68).

The findings on cyanide doped alkali halides are summarized as follows: The CN^- ions in potassium salts and in RbCl have a surprisingly low barrier to rotation, i.e., they behave like a dilute gas of free molecules down to temperatures as low as 50°K, except for the absence of translational motion. The lowest, perturbed rotor states can be described as librational states. Their energies are of the order of 10 cm^{-1} (~15°K), and they are split due to tunneling. The tunnel splitting of the librational ground state is of order 1 cm^{-1} (~1.5°K). A complete list of the tunneling states will be given later in Fig. 37. In sodium salts, the barrier to rotation is considerably higher, causing the molecule to be frozen-in even at 300°K. No evidence for tunnel splitting has been found in these hosts.

Note added in Proof: Recent studies of the rotational Raman effect in CN^- doped alkali halides by Callender and Pershan [R. H. Callender, Ph.D. Thesis, Harvard University, 1969 and R. H. Callender and P. S. Pershan, Phys. Rev. Letters **23,** 947 (1969)] are in essential agreement with the results discussed above. In NaCl:CN they have observed a librational splitting of 54 cm^{-1} which yields a value of the Devonshire potential parameter $\tilde{K} \approx 100\, \tilde{B} = 125$ cm^{-1}, and a tunnel splitting of less than 10^{-1} cm^{-1}.

Phonon resonant scattering is observed in those hosts in which the barrier to rotation is low. The temperature of the lower dip in the thermal conductivity curves is close to the tunnel splitting (divided by Boltzmann's constant). The dips at higher temperature correspond to energies of the librational or rotational states near the potential barrier. It has been shown that the latter assignment is correct, and that the librational states do not scatter phonons (SN66, NSP66, Po63), but this question shall not concern us in this paper. The resonant scattering by the tunneling states will be discussed in Chapter VI.A.

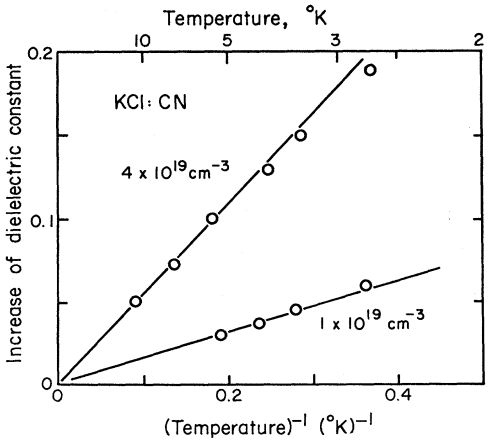

FIG. 15. Excess dielectric constant in KCl:CN, after Sack and Moriarty (SM65), determined with an ac method, frequencies between 10^2 and 10^5 sec^{-1}. No dependence on the frequencies was found.

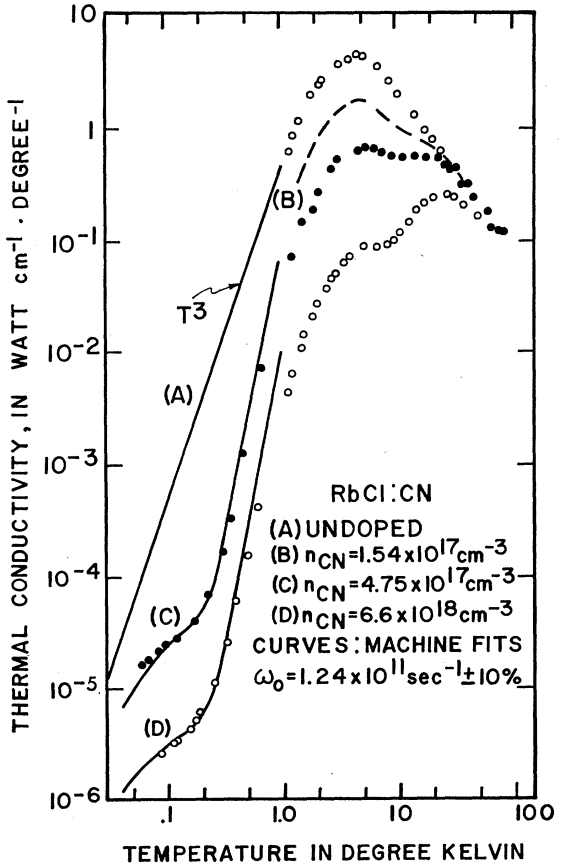

FIG. 16. Thermal conductivity of RbCl containing various CN^- concentrations. Solid lines are machine calculations which will be used in VI.A. After Harrison *et al.* (HPP68).

The discussion of the perturbed rotor states using the Devonshire potential appears to be highly successful. This potential, however, is very simple and one should therefore ask whether the agreement between theory and experiment is fortuitous, or whether the simplifying assumptions are indeed justified. The study of these questions is the subject of the next section.

B. The CN^- Ion. Refinements of the Theory

In using the Devonshire potential to calculate the perturbed rotor states of the impurity ion, the tacit assumptions made are: (1) that the neighboring ions are stationary, (2) that the potential has full octahedral symmetry undistorted by random internal stresses or by the impurity itself, and (3) that the motion of the impurity ion can be considered as a purely rotational one described by the two spherical coordinates θ and ϕ

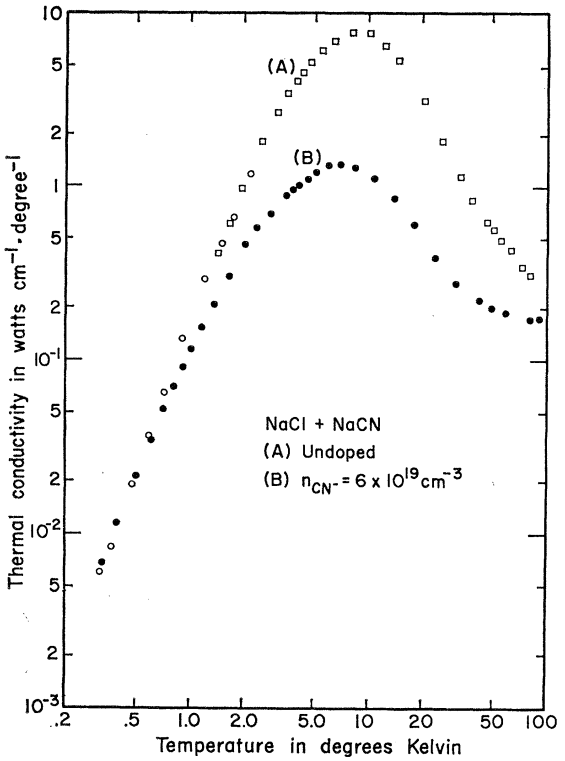

FIG. 17. Thermal conductivity of NaCl:CN. A: undoped; B: 6×10^{19} cm^{-3} CN^- ions and 5×10^{17} cm^{-3} NCO^- ions (SN66).

alone. The experimental results presented in this section require a closer inspection of these assumptions, in particular of the second one.

The rotational constants B of the CN^- ion, derived from the infrared rotation–vibration spectrum at high temperatures, are somewhat smaller in the KBr, KI, and RbCl host lattices than in KCl (SN66), which suggests an increase of the rotational inertia I, as might be expected if the ion was not rotating by itself, but, in a simple-minded picture, was dragging along some of its neighbors. This observation demonstrates that a separation of the motion of the lattice and of the impurity ion may lead to noticeable discrepancies between theory and experiment, in this case, regarding the higher rotational states of the defect.

The experiments described below will deal specifically with the tunneling states. The specific heat anomaly of the tunneling states in RbCl:CN is shown in Fig. 18. It consists of two maxima. The one at low temperatures corresponds to a splitting slightly larger than 0.1 cm^{-1}, and the one at higher temperatures to a splitting of about 0.6 cm^{-1}. A similar shape of the anomaly was found in KBr:CN and KI:CN, although in these hosts the separation of the two maxima is less pronounced (PPHN70). This separation indicates that the splitting between the lowest and highest excited tunneling states is about 5 times larger than the splitting between the lowest and the first excited tunneling states. This is incompatible with the Devonshire model, as shown in Fig. 5. Also note that even in KCl:CN the specific heat anomaly is slightly broader than predicted, see Fig. 14.

An additional complexity arose in the study of the electric field induced dichroism of the CN^- stretching vibration (PN68). For a dc field E_{appl} applied parallel to the electric field vector E_{light}, the absorption constant α was found to decrease, see Fig. 19, without measurable change of the line shape. Similar results were obtained for KCl, KBr, KI, and RbCl hosts. This decrease of the absorption is contrary to what is expected for classical dipole oscillators, which would absorb more light in such a field configuration, and also disagrees with a quantum mechanical calculation based on the tunneling states of the diatomic molecule in a Devonshire potential.

These measurements demonstrated that both the tunnel splittings and the sign of the dichroism depend very critically on details of the crystal field around the defect. Pompi and Narayanamurti (PN68) showed that a small tetragonal distortion of the cubic field can cause one of the T_{1u} states to drop very close to the ground state, see Fig. 20, and that this will cause an additional low-temperature maximum in the specific heat. In an electric field these two states separate again. The depopulation of the ir-active levels $2A_1$* and $3A_1$* of higher oscillator strength, together with the increase of

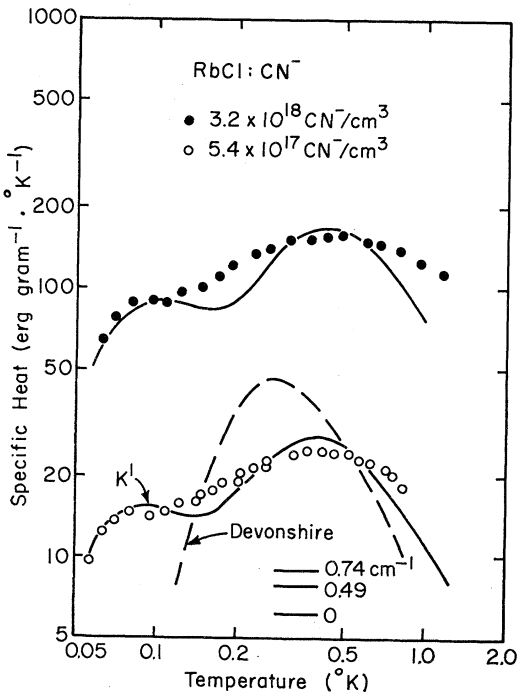

FIG. 18. Specific-heat anomaly in RbCl:CN, after Harrison *et al.* (HPP68). The anomalies scale with CN^- concentration. The dashed curve is the Schottky anomaly predicted from near-infrared work on the basis of the Devonshire model. The solid curves are anomalies computed with a tetragonally distorted Devonshire potential, after Pompi and Narayanamurti (PN68); see also Fig. 20.

the population of the $1A_1^*$ level of lower oscillator strength, and of the ir-inactive E level gives rise to a small *decrease* in the optical absorption for light polarized parallel to the applied field, in agreement with the experiment.

For the calculation a potential of the form

$$V = V_{\text{Dev}} + (4\pi)^{1/2} K' Y_2^0 \qquad (15)$$

was used, where V_{Dev} is the Devonshire potential of cubic symmetry, Eq. (5), and the second term has tetragonal symmetry. K' was adjusted to obtain a good fit to the specific heat data, see Figs. 14 and 18 for the KCl and RbCl hosts, respectively. K' is relatively small, $0.04K$, $0.1K$, and $0.03K$ for KCl, KBr, and RbCl, respectively. A positive K' implies that the cavity is elongated along one [100] direction. A summary of K, K', and the tunnel splittings in the different hosts can be found in Chapter VI, Fig. 37. With these K', the second-order Stark effect and the induced dichroism were calculated. The dichroism was of the correct sign and its magnitude agreed with the observed one. The origin of the distortion is not known. Both random internal strains and a distortion by the molecule itself have been considered (PN68).

The important result of this work is that the Devonshire model comes remarkably close to describing the motional states of the CN^- ion in different alkali halides, and that the rather striking discrepancies mentioned above can all be accounted for by the addition of a relatively small tetragonal term (as caused for instance by an internal stress) to the cubic potential.

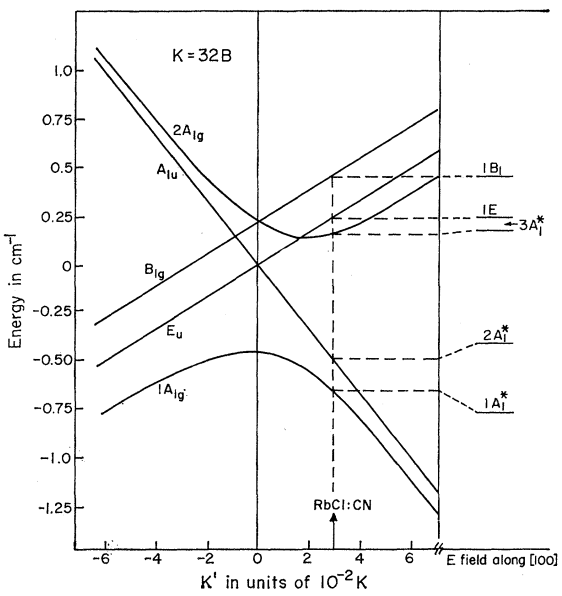

FIG. 20. The six lowest motional states (tunneling states) of a diatomic molecule in a crystal field given by Eq. (15), as a function of the parameter K' of the tetragonal distortion, for $K = 32B$. The dashed line marks the distortion $K' = 0.03K$, which fits the specific heat anomaly of RbCl:CN. Rotational constant $\tilde{B} = 1.1$ cm^{-1}. Positive K' means that two of the six potential minima are lower than the other four. On the right of the graph is shown schematically how the energy states change in an applied electric field. The levels marked with an asterisk are infrared active for $E_{\text{appl}} \parallel E_{\text{ir}}$ (PN68).

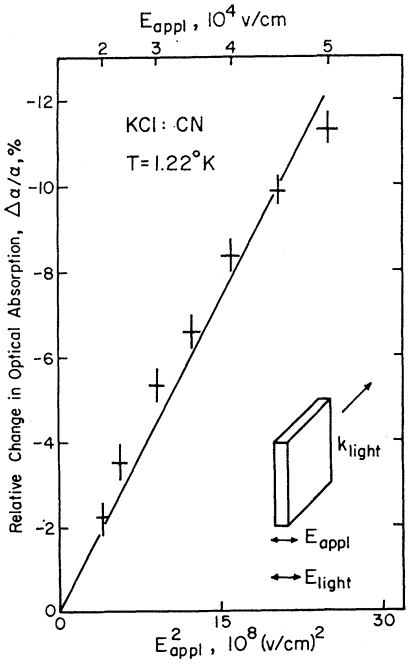

FIG. 19. Electric field induced dichroism of the CN^- stretching vibration in KCl:CN ($\lambda^{-1} = 2089$ cm^{-1}). Note that the absorption constant α decreases with increasing electric field, contrary to the expectation based on classical arguments. $n \sim 5 \times 10^{18}$ cm^{-3}, $T = 1.22$°K (PN68).

In studies of the paraelectric resonance in RbCl:CN at microwave frequencies of 8.1 and 10.2 GHz, Dreyfus (Dr68) observed more transitions than were compatible with the Devonshire model for both $K > 0$ and $K < 0$. He explained his data with the assumption that the CN^- ion had potential minima in the 12 ⟨110⟩ directions. The specific-heat anomaly predicted by this model, however, does not agree with the experiment; it fails to show the high-temperature peak (PPHN70). An attempt to explain the paraelectric data using the distorted Devonshire potential has not been made but appears to be promising.

Finally, we want to mention an experiment on CN^- ions whose interpretation still presents a major puzzle. Byer and Sack (BS68) investigated ultrasonic velocity and attenuation in CN doped KCl, KBr, KI, and NaCl in the frequency range 10–200 MHz at temperatures above 1.6°K. Using classical continuum elastic dipole theory (NH65), they were unable to explain their results with an elastic dipole tensor represented by an ellipsoid of revolution and with the CN^- axis having ⟨100⟩ equilibrium orientations. They assumed instead that because of elastic deformations of the surrounding cavity, the long axis of the elastic tensor points in a ⟨110⟩ direction, while the electric dipole, pointing in the C–N internuclear axis, has equilibrium orientations

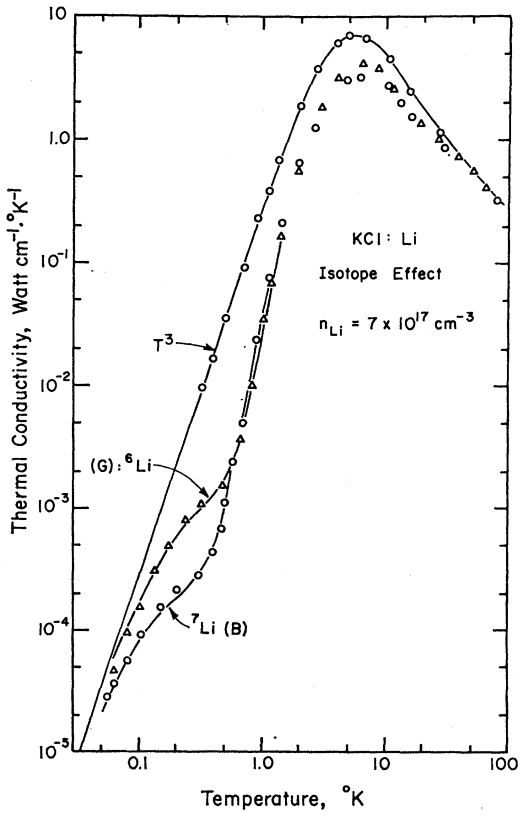

FIG. 21. Isotope effect on the low-temperature phonon resonance scattering in KCl:^{7}Li and LCl:^{6}Li. After Peressini *et al.* (PHP69). The measurements of pure KCl actually have been extended to 0.08°K, see Fig. 8, and the data follow a straight line which varies as T^3.

along ⟨100⟩. These peculiar elastic properties are probably related to the nonvanishing stress induced dichroism for [111] stress noted in Fig. 13. It would be of interest to attempt an explanation of these observations with the model of a tetragonal distortion of the Devonshire potential.

C. The Li^+ Ion

During a systematic search for impurity modes through measurements of the thermal conductivity in single crystals of alkali halides, Baumann *et al.* (Ba64, BHPS67) noticed a low-frequency resonance in KCl:Li. Figure 21 shows some recent data (PHP69). In crystals containing the naturally abundant ^{7}Li isotope, the dip in the conductivity curve occurs around 0.5°K. For the lighter ^{6}Li isotope, the dip is shifted to higher temperatures. This shift can be demonstrated even more clearly by plotting the average phonon relaxation rate $\bar{\tau}^{-1}$, determined from the expression of the thermal conductivity

$$K(T)=\tfrac{1}{3}C_v v\bar{l}=\tfrac{1}{3}C_v v^2\bar{\tau}, \qquad (16)$$

where C_v is the specific heat of the host, v the velocity of sound, and $\bar{l}$ the average phonon mean free path (Ki62).

At low temperatures, $K(T)\propto T^3$ in the pure crystal (boundary limited conductivity), $C_v\propto T^3$, and $\bar{l}=l_{bd}$ is frequency independent and of the order of the crystal diameter. In the doped crystal, the specific heat C_v connected with the phonons carrying the heat, and the phonon velocity v remain unchanged in the first approximation, and thus $\bar{\tau}^{-1}$ can be determined by comparing the conductivities of the pure and the doped crystals:

$$\bar{\tau}^{-1}=\bar{\tau}_{bd}^{-1}(K_{\text{pure}}/K_{\text{doped}}). \qquad (17)$$

This average relaxation rate $\bar{\tau}^{-1}$ is a rather sharply peaked function, see Fig. 22. In KCl:Li^7, it peaks at $T_7=0.44$°K, and in KCl:Li^6, at $T_6=0.62$°K, i.e., at a 40% higher temperature.

The isotope effect demonstrates that the resonance scattering is caused by some motional states of the lithium ions, but its magnitude speaks against such motions as an Einstein oscillator or a quantum mechanical particle in a box, which have isotopic shifts of 8% or 16%, respectively [$(7/6)^{1/2}$ and $(7/6)$]. The striking similarity of the low-temperature thermal conductivity of KCl:Li and of crystals containing tunneling molecules (see Fig. 8 and in particular Fig. 16), together with the large impurity induced polarizability demonstrated through dielectric (SM65) and electrocaloric measurements led to the suggestion that the small Li^+ ion can occupy several equivalent potential minima inside the potassium vacancy, between which it can tunnel (LP65). This model has since been tested in detail both theoretically and experimentally, and the lithium tunneling states, which have been clearly identified as such, now belong to the most thoroughly studied impurity modes in solids. The equilibrium positions within the potassium

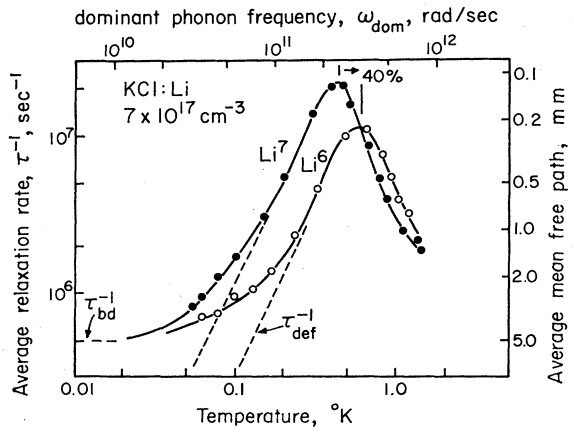

FIG. 22. Average phonon relaxation rate $\bar{\tau}^{-1}$ and mean free path $\bar{l}$ as determined from thermal conductivity, Fig. 21, using Eq. (17); (τ_{bd}^{-1}), the boundary, scattering rate, is 5×10^5 sec^{-1} for a sample of 5-mm-square cross section in agreement with the theory. The dashed lines, marked $\bar{\tau}_{\text{def}}^{-1}$, were obtained by subtracting τ_{bd}^{-1} from $\bar{\tau}^{-1}$; $\bar{\tau}_{\text{def}}^{-1}$ varies as T^2. The dominant phonon frequency ω_{dom} will be needed in Chapter VI. It is defined as the frequency of those phonons which contribute most to the specific heat at any given temperature in the Debye approximation. $\omega_{\text{dom}}=(2\times9\times10^{10}$ rad/sec) (T°K^{-1}), or $\hbar\omega_{\text{dom}}=4.3\,k_BT$, or 1°K corresponds to 3 cm^{-1} in wavenumbers. See also later, Fig. 35.

cavity and the paths along which the lithium ion tunnels are shown in Fig. 23. Figures 24 and 25 give the energies of the tunneling states in zero field and in applied electric and stress fields, as derived from the investigations to be reviewed in the following.

The theoretical aspects of the off-center ions have recently been reviewed by Smoluchowski (Sm69), and we therefore restrict ourselves to a brief summary thereof.

It was shown by Matthew (Ma65) that if a small ion substitutes for a larger one in an ionic crystal, the induced electric dipoles together with the decreased repulsive forces could indeed cause highly asymmetric equilibrium configurations. The shape of the potential was investigated in several calculations (DHSW66, QD67, WHDS67). It was shown that through a proper choice of the repulsive and polarization forces, it was possible to derive a potential which had eight minima in the ⟨111⟩ directions, in agreement with the experimental findings in KCl:Li. These calculations of the lattice energy have demonstrated that a comparison of the potential derived from experiment with that deduced from the theory will provide a very sensitive test for the different models of the forces of interaction between ions in solids.

The tunneling states for a three-dimensional harmonic oscillator in eight identical, rigid spherical potential wells, corresponding to the situation shown in Fig. 23, were calculated by Krumhansl and co-workers (GBK67, BGKM66) (see also Chapter III). These authors also studied the influence of an applied electric field and of uniaxial stress on the tunneling states. The energies W_i of the eight states in an electric field E are given by the following expressions (HPP68a) (Δ_0 is the zero-field tunnel splitting, p_0 is the dipole moment, and the indices are the same as in Fig. 24):

For $E \parallel \langle 111 \rangle$:

$$W_{1,8} = \mp[(\tfrac{3}{2}\Delta_0)^2 + p_0^2E^2]^{1/2}, \tag{18}$$

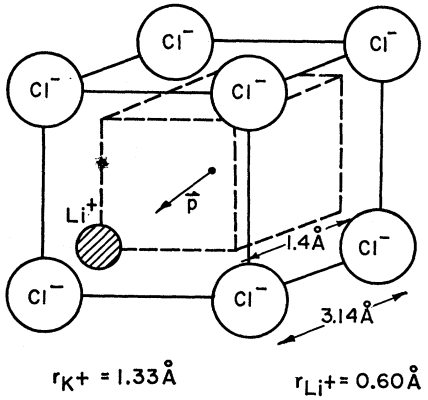

FIG. 23. KCl:Li. The eight potential wells lie at the corners of a cube of 1.4 Å edge length. The Li^+ tunnels predominantly along the dashed cube edges. The Cl^- ions at the centers of the large cube faces have been omitted for clarity. p indicates the electric dipole moment.

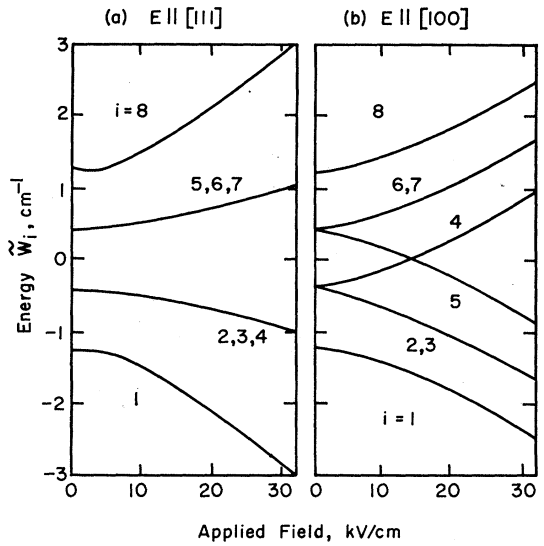

FIG. 24. Influence of electric field on the Li^+ tunneling states in KCl:^{7}Li. The curves are labeled with the indices used for W_i in Eqs. (18)–(22). The electric dipole moment p_0 used for the calculation is 6 D (uncorrected) (HPP68a).

and

$$W_{2-4;\,5-7} = \mp[(\tfrac{1}{2}\Delta_0)^2 + \tfrac{1}{3}p_0^2E^2]^{1/2}. \tag{19}$$

For $E \parallel \langle 100 \rangle$:

$$W_1 = -\Delta_0 - [(\tfrac{1}{2}\Delta_0)^2 + \tfrac{1}{3}p_0^2E^2]^{1/2}, \qquad W_i = -W_1, \tag{20}$$

$$W_{2,3} = -[(\tfrac{1}{2}\Delta_0)^2 + \tfrac{1}{3}p_0^2E^2]^{1/2}, \qquad W_{6,7} = W_{2,3}, \tag{21}$$

$$W_4 = -\Delta_0 + [(\tfrac{1}{2}\Delta_0)^2 + \tfrac{1}{3}p_0^2E^2]^{1/2}, \qquad W_5 = -W_4. \tag{22}$$

Now we turn to the experimental work. In measurements of the ac dielectric constant (SM65) above 1°K it was noticed that the low-temperature polarizability of KCl was greatly increased by the addition of small amounts of LiCl. Electric cooling (LP65) achieved with KCl:Li could be explained with an excess polarization P following a Langevin–Debye law:

$$P = n_{\mathrm{Li}}p_0^2E/3k_BT, \tag{23}$$

where n_{Li} is the lithium concentration, determined spectrochemically, p_0 an electric dipole moment, E the applied electric field, k_B Boltzmann's constant, and T the temperature. The value of p_0 was found to be 5.5 D = 1.14e Å (uncorrected for local electric field), with an error of about 10%, caused mainly by the error in n_{Li}. It has since been shown (HPP68a) that a polarizable system of tunneling states will also show a polarization of the form given in Eq. (23), provided $k_BT > W_2 \sim \Delta_0/2$ (at low fields). Hence the dielectric and electrocaloric work established that $\Delta_0 < 2$°K $k_B(\sim 3\ \mathrm{cm}^{-1})$.

For a more quantitative understanding of the tunneling states, the equilibrium orientations, i.e., the directions in which the potential minima occur, had to be established. This was done through measurements of

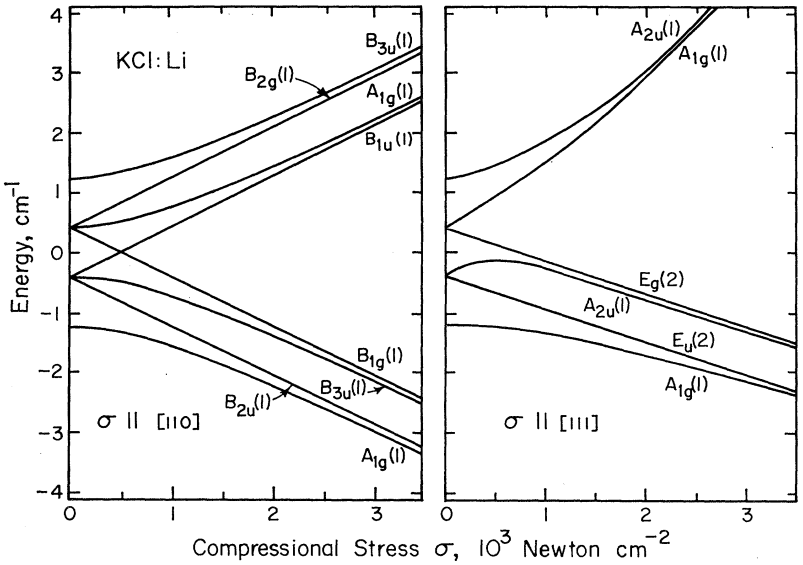

FIG. 25. Influence of compressional stress on the tunneling states in KCl:Li. In his calculation, Alderman assumed that the stress does not change the overlap between the localized pocket states. Consequently, stress $\sigma \parallel [100]$ does not change the tunnel states at all. The elastic dipole moment p_λ used for the calculation is 3.8×10^{-24} cm^3. 10^3 N cm$^{-2}\approx100$ atm (Al69, AC69).

sound velocity (BS68b) and of nuclear magnetic resonance (AC69, Al69). Figure 26 shows the relative change of the sound velocity in KCl:Li for shear waves propagated along a [110] direction; in curves A and B the wave was polarized in the [001] direction (T_{2g} mode); in curve C it was polarized in [1$\bar{1}$0] (E_g mode). In cases A and B, the velocity of propagation $v_{A,B}$ is given by

$$v_{A,B}^{-2}=\rho S_{44}, \tag{24}$$

where ρ is the mass density of crystal and S_{44} is the elastic compliance. In case C, the velocity of propagation is

$$v_C^{-2}=2\rho(S_{11}-S_{12}). \tag{25}$$

Introduction of the defect changed S_{44}, while leaving $(S_{11}-S_{12})$ unaltered. According to classical elastic dipole theory (NH63, NH65), this means that the equilibrium orientations of the dipole point along the eight ⟨111⟩ cube diagonals.

The same conclusion was reached in measurements of the stress induced first-order electric quadrupole splitting of the ^{7}Li nuclear magnetic resonance line (AC69, Al69). Figure 27, top, shows the two sidebands of the NMR Zeeman line at 16 MHz. They result from a perturbation of the Zeeman levels, if the nucleus with quadrupole moment eQ is localized in an electric field gradient. In this experiment, the localization was accomplished by uniaxial stress, and Fig. 27, bottom, shows the quadrupole splitting f_Q as a function of temperature and stress. The quadrupole splitting depends on the crystallographic directions along which the uniaxial stress and the magnetic field point. By studying this angular dependence, Alderman and Cotts were able to show that only potential minima along ⟨111⟩ were compatible with their results.

The NMR measurements were also used to determine the electric quadrupole interaction energy e^2Qq_0 of a ^{7}Li nucleus localized in one well. The experimental value, $h\times7.1\times10^4$ sec^{-1}, agreed closely with the energy derived from the calculated crystal field (QD67), $(e^2Qq_0)_{\text{theory}}=h\times8.5\times10^4$ sec^{-1}.

Alderman and Cotts also measured the influence of uniaxial stress on the energy of the tunneling states, and by fitting their data to the theory (Fig. 27) they determined the T_{2g} stress Hamiltonian coefficient $\tilde{p}_\lambda$ (which they called B) to

$$\tilde{p}_\lambda=8.2\times10^{-3}\text{ cm}^{-1}/\text{bar}, \tag{26}$$

(energy measured in wavenumbers), or

$$p_\lambda=4\times10^{-24}\text{ cm}^3, \tag{27}$$

in agreement with the value determined by Byer and Sack (BS68) using classical elastic dipole theory. Note that in the classical theory p_λ, the elastic dipole moment, is usually called α or $(\lambda_1-\lambda_2)v$, where λ_1 and λ_2 are the principal values of the elastic dipole moment tensor,

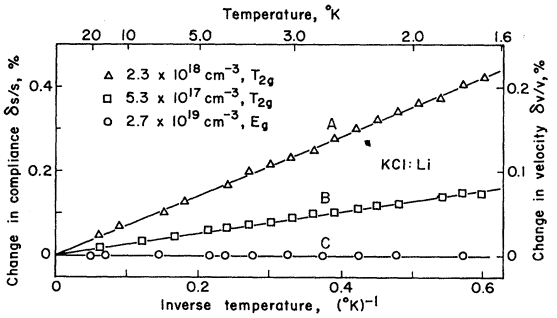

FIG. 26. KCl:Li. Relative change of the elastic compliance $S(T_{2g})=S_{44}$ for a shear wave propagating in a [100] direction with [001] polarization (T_{2g} mode). A shear mode propagating in [110] but polarized parallel to [1$\bar{1}$0] (E_g mode) is not influenced by the lithium ions, see open circles. After Byer and Sack (BS68).

and v is the atomic volume of the host crystal. The energy difference W between the two dipole orientations parallel and perpendicular to the stress is given by

$$W = p_\lambda \sigma, \tag{28}$$

where σ is the applied stress.

In both the ultrasonic and the magnetic resonance studies no coupling of the tunneling states to a tetragonal stress (E_θ) was observed. We shall return to this important point in the discussion of the phonon scattering by the tunneling states.

Lakatos and Sack (LS66) measured the temperature dependence of the real and imaginary parts of the dielectric constant, κ' and κ'', in KCl:Li at 22, 24, and 26 GHz, and found a zero-field tunnel splitting of 24 GHz (0.81 cm^{-1}). This value was close to the one determined from an extension of the measurements of the ac dielectric constant to lower temperatures (BS66b), which was 0.76 cm^{-1}.

The specific-heat anomaly associated with the lithium tunneling states was studied by Wielinga *et al.* (WMH66) and by Harrison *et al.* (HPP68). Some of the data are shown in Figs. 28 and 29. Over a wide concentration range, the total entropy agrees closely

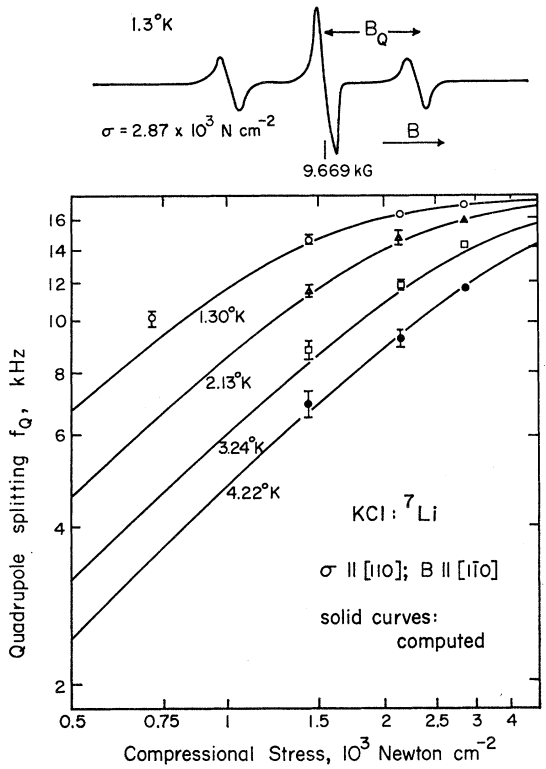

FIG. 27. Stress induced quadrupole splitting of the ^{7}Li nuclear magnetic resonance line. Top: spectrum at 1.3°K, stress σ || [110], B || [1$\bar{1}$0], $\sigma = 2.87\times10^8$ N cm^{-2} = 287 bar. $n_{Li}\sim10^{18}$ cm^{-3}. The quadrupole splitting f_Q is determined from the magnetic field change B_Q with the conversion factor $f_Q = B_Q$ 1.6547 kHz/G. In top picture, $B_Q\sim10$ G. Bottom: stress and temperature dependence of f_Q. At decreasing temperature the stress induced localization of the Li ion increases (Al69, AC69).

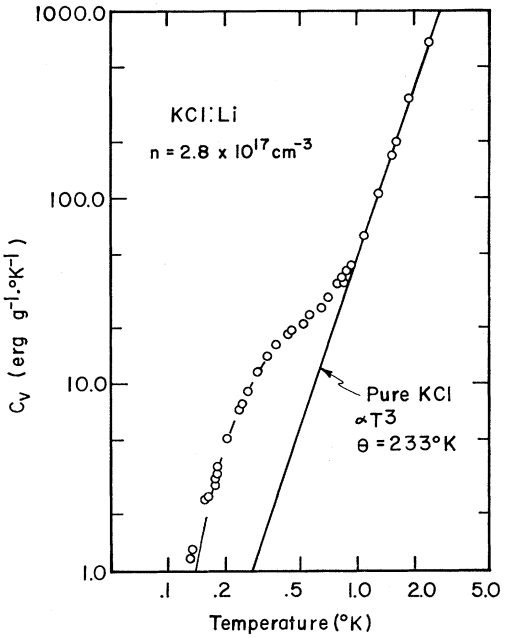

FIG. 28. Specific heat of KCl:Li between 0.14 and 2.5°K. $n_{Li} = 2.8\times10^{17}$ cm^{-3}. Normal isotopic mixture (92.6% ^{7}Li, 7.4% ^{6}Li). The solid line is the specific heat of pure KCl, $C_v = 46$ erg gram^{-1}·K^{-4} T^3, $\theta = 233$°K. The curve drawn through the low-temperature points is the calculated low-temperature exponential portion of a Schottky specific-heat anomaly, with an "activation energy" of 10^{-4} eV. The full Schottky anomaly is shown in Fig. 29. (HPP68a).

with the predicted value of

$$\Delta S = n_{Li} k_B \ln 8. \tag{29}$$

The excess specific heat can be well fitted with a Schottky (HPP68) anomaly calculated on the basis of the theoretical model, with a zero-field splitting $\Delta_0^7 = 1.0\times10^{-4}$ eV (0.82 cm^{-1}) ±5% for the ^{7}Li isotope.

For KCl doped with ^{6}Li, the shape of the anomaly remains unaltered, but the entire anomaly is shifted up in temperature by 40±5%, i.e., by the same amount as was observed in thermal conductivity (PHP69). This large isotope effect provides strong evidence that these motional states are caused by tunneling, as was shown with the two following simple calculations: (a) KCl:^{7}Li has a far-infrared absorption band at 42 cm^{-1} (CNS67). Assume a one-dimensional, double-well, harmonic oscillator, which has the mass of the ^{7}Li ion, oscillates with a frequency of 42 cm^{-1}, and has a ground-state tunnel splitting of 0.82 cm^{-1}. If, in such an oscillator, the ^{7}Li is replaced by ^{6}Li, the tunnel splitting increases by 59% (HPP68b). (b) In a three-dimensional calculation, the Li^+ ion can be pictured as performing a quasirotational motion with the rotational inertia $I = r_0^2 m$, where r_0 is the separation of the potential wells from the cavity center, and m is the mass of the ion (see also Chapter III). In the Devonshire model, the far-infrared absorption peaked at 42 cm^{-1} corresponds to an excitation of a librational state. In this

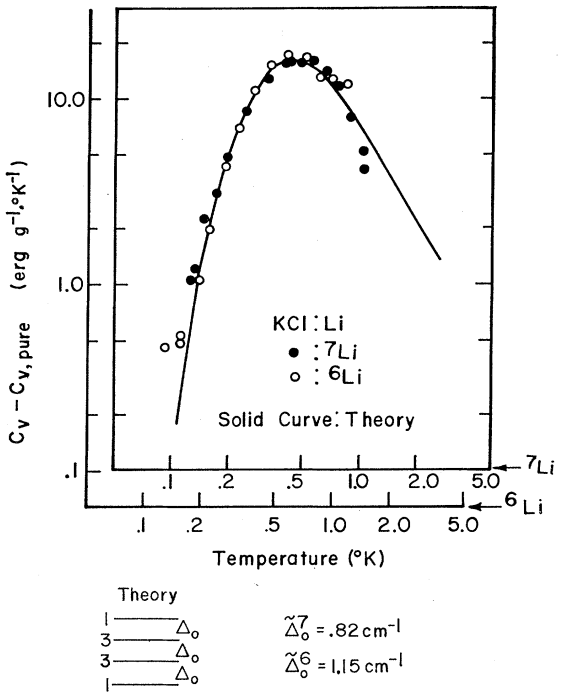

FIG. 29. Excess specific heat caused by the tunneling states of LiCl dissolved in KCl, and the influence of the isotopic mass of the lithium ion on it. Closed circles: ^{7}Li ($n_{Li}=2.8\times10^{17}$ cm^{-3}, actually normal isotopic mixture, 92.6% ^{7}Li, 7.4% ^{6}Li); open circles: isotopically pure ^{6}Li ($n_{Li}=2.44\times10^{17}$ cm^{-3}). Concentrations determined with a spectrochemical analysis, estimated error 30%. Note that the anomaly for ^{6}Li occurs at 40% higher temperatures than that for ^{7}Li, indicating a 40% larger tunnel splitting for ^{6}Li. In order to demonstrate this clearly, the temperature scale used for the ^{6}Li anomaly (lower scale) was shifted to the left by 40% relative to that used for the ^{7}Li anomaly, until the two anomalies coincided exactly. Doubly logarithmic plot. The solid curve was computed for a system of four equally spaced levels of spacing Δ_0 with degeneracies 1, 3, 3, and 1, according to the model of Gomez *et al.* (GBK67, BGKM66), and $n_{Li}=1.6\times10^{17}$ cm^{-3}. From the best fit to the experimental data, one finds $\tilde{\Delta}_0^7=0.82$ cm^{-1}, $\tilde{\Delta}_0^6=1.15$ cm$^{-1}=1.4\times\tilde{\Delta}_0^7$ (HPP68a).

model, the increase in tunnel splitting in going from ^{7}Li to ^{6}Li is 54% (HPP68a).

In view of the simplicity of both of these models, these isotopic shifts are in very good agreement with the experimental shift of 40%. The Devonshire model also allows one to determine the rotational inertia of the dumbbell and from it the separation of the potential wells from the cavity center. It was (HPP68a)

$$r_0=1.2\ \text{Å}, \tag{30}$$

in agreement with the displacement calculated from interatomic potentials; Wilson *et al.* (WHDS67) found $r_0=1.16$ Å, and Quigley and Das (QD67) found $r_0=0.6$ Å.

An electric field changes the tunnel splitting, as indicated in Fig. 24. Harrison *et al.* (HPP68a) studied this with specific-heat measurements and found that the change observed in an electric field applied along different crystallographic directions agreed with the theoretical model. From their measurements, a dipole moment p_0 could be determined which did not require a knowledge of the lithium concentration. They found (uncorrected for local fields):

$$p_0=6.0\ \text{D}=1.24e\ \text{Å}, \tag{31}$$

with an accuracy of 10%. From this, an effective charge e^* of the lithium ion was determined through the relation $p_0=r_0e^*$. It was found that e^* was about 0.5 of an electronic charge. This is to be compared with an effective electric charge e^* for pure alkali halide crystals, determined by Szigeti to lie between 0.7 and 0.9e (see, for instance, Ki62, Chap. 7).

Herendeen and Silsbee (He68, HS69) and Höcherl *et al.* (HW68) studied the lithium tunneling states through paraelectric resonance at the microwave frequencies of 63, 24, and 9, and of 35 Ghz, respectively. Resonance spectra obtained for different sample orientations and frequencies agree with the model of a ⟨111⟩ defect. Figure 30, top, shows a spectrum obtained by Herendeen and Silsbee (He68, HS69) on KCl:^{7}Li. The derivative of the microwave absorption spectrum indicates one strong and two weak transitions, at the fields E_1, E_2 and E_3. The absorption at E_1 corresponds to the three degenerate dipole allowed transitions as indicated in Fig. 30, bottom. The weaker absorption bands result from forbidden transitions which become allowed because of random internal strains with a rms strain energy of $h\times7\times10^9$ sec^{-1} (0.23 cm^{-1}). The resonance measurements also allow a precise determination of the lithium dipole moment p_0, $p_0=(5.6\pm0.3)$ D, in good agreement with the dipole moment deter-

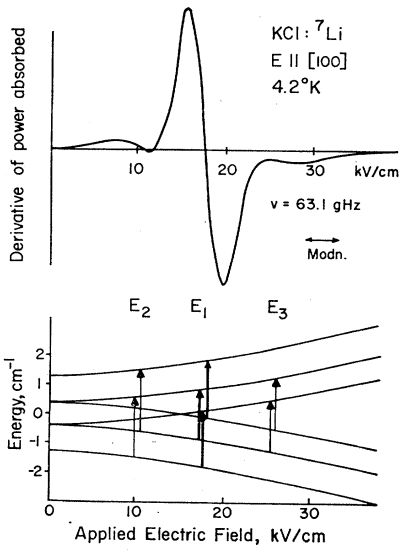

FIG. 30. KCl:Li. Paraelectric resonance. Top: spectrum for both the dc and the microwave electric field parallel to [100]. Transitions are observed at the fields E_1, E_2, and E_3. Bottom: the strong absorption at E_1 is ascribed to the three dipole allowed transitions (heavy arrows). The weaker transitions at E_2 and E_3 (light arrows) are allowed only because of random internal strains. After Herendeen and Silsbee (He68, HS69).

mined through specific-heat and electrocaloric measurements. No variation of the dipole moment with the isotopic mass of the lithium ion was found (He68, HS69). The zero-field splitting determined from this work, 0.77 ± 0.03 and 1.07 ± 0.04 cm^{-1} for ^{7}Li and ^{6}Li, respectively, agrees well with the previously determined values of 0.82 and 1.15 cm^{-1}, respectively.

A consequence of the model of a quasirotational tunneling motion along the cube edge between adjacent wells (Fig. 23) is that in zero field the tunneling states are separated by equal energies Δ_0. The paraelectric resonance spectra (He68, HS69) have shown just such a splitting and therefore provide evidence for the correctness of the theoretical model.

Optical absorption by the tunneling states was observed in far-infrared measurements by Kirby and Sievers (KS69). In an applied electric field up to 100 kV/cm, they observed a single line whose frequency varied linearly with field ($p_0=5.5$ D) and which they ascribed to the strong transition observed in paraelectric resonance. Because of the sensitivity of their measurement, the weaker absorptions were not found.

We turn to the discussion of the width of the tunneling levels, which has been determined in several experiments: The shapes of the observed and the computed specific-heat anomalies (HPP68a) agree almost perfectly (see Fig. 29). Hence, the effect of a distortion of the potential or any level broadening must be small enough as to be indiscernible at these concentrations (2.8×10^{17} cm^{-3}). It was estimated that a broadening of the lowest two levels by more than $0.2\Delta_0$ would have been observed in these measurements, and therefore their width (full width at half-maximum) must be less than ~0.2 cm^{-1}. From paraelectric resonance experiments at 4.2°K and with $n_{Li}\leq10^{17}$ cm^{-3}, a rms width (full width between inflection points) of 0.5 cm^{-1} was determined (He68, HS69, HW68) with no significant change after annealing at 650°C (He68, HS69). With $n_{Li}=4.6\times10^{17}$ cm^{-3}, Kirby and Sievers (KS69) found a width (full width at half-maximum) of 0.6 cm^{-1} in far-infrared absorption, independent of temperature between 1.2 and 4.2°K. From nuclear magnetic resonance, Alderman and Cotts (AC69, Al69) determined a rms width of 0.2 cm^{-1} for $n_{Li}=8\times10^{17}$ cm^{-3}. Finally, Lakatos and Sack (LS66) found a width of 0.2 cm^{-1} from microwave dielectric measurements at helium temperature for $n_{Li}\sim4\times10^{17}$ cm^{-3}. Note that the width determined in each experiment also depends on the line shape used in evaluating the data. But regardless of this ambiguity, the width of the tunneling states is 0.3 cm^{-1} to within a factor of 2.

Because of the temperature independence of the line width (KS69), the lifetime of the tunneling states can be ruled out as cause for the broadening. Random internal stresses of a magnitude between 60 and 1000 N cm^{-2} are more likely (AC69, Al69). Such stresses have been postulated repeatedly in alkali halides (Su64, SN66). Herendeen and Silsbee (He68, HS69) also considered random internal electric fields as a cause for the line broadening of the allowed transition in the [100] field case (E_1 in Fig. 30), since they found that for this field direction random stresses can change the line width only in second order. They found that a small internal field, equivalent to an applied field $E=1.7$ kV/cm, could explain the observed linewidth. The origin of the field is unknown; it is, however, too large to be caused by neighboring Li dipoles at the concentration studied, if the ions are assumed to be randomly distributed.

At concentrations exceeding 10^{18} cm^{-3}, the tunneling levels broaden rapidly, as was first noticed through a broadening of the specific heat anomaly (HPP68a) for $n_{Li}=3\times10^{18}$ cm^{-3}, the half-width of the levels was found to be $\Delta_0/2=0.4$ cm^{-1}. For $n_{Li}=5\times10^{18}$ cm^{-3}, Kirby and Sievers (KS69) found that the far-infrared absorption band caused by the tunneling states had a half-width ~2 cm^{-1}, independent of temperature between 1.2 and 4.2°K. This increased width could be explained through the polarizing effect by neighboring dipoles.

D. The OH^- Ion

The substitution of the OH^- ion for a halogen ion is a very common impurity in alkali halide crystals. It was identified by Etzel and Patterson (EP58) and by Rolfe (Ro58) through its ultraviolet absorption caused by an electronic transition. In intentionally OH^- doped KCl crystals Fritz *et al.* (FAL63) observed an infrared absorption whose frequency lies in the region of the hydrogen stretching vibration and which scaled with the ultraviolet absorption. The influence of the stretching vibration on the ultraviolet absorption and luminescence has also been observed (Fi64, PK65, Ko65).

In nominally pure NaCl crystals, Klein (Kl61) observed that the thermal conductivity at low temperatures ($T<10$°K) was several orders of magnitude smaller than expected if the conductivity were limited by boundary scattering alone. He was able to correlate the excess thermal resistance with the ultraviolet absorption ascribed to the OH^- ion. He also demonstrated that by intentional doping of carefully purified (WW35) NaCl with NaOH this excess resistance could be enhanced.

Klein attempted to explain the strong phonon scattering as a resonance interaction with some rotational or tunneling states of the molecular impurity (Kl61, Kl61a). Brugger and Mason (BM61, BFK67) showed that the same impurity also attenuated ultrasound in KCl and NaCl (frequencies between 0.5 and 500 MHz), and explained this as a reorientation of the impurity ion via a relaxation process. Direct evidence for the high rotational mobility of the OH^- ion at low temperatures was obtained through measurements of electric field (Kl64) and stress (HL65, Ha66) induced dichroism of the ultraviolet absorption band in several OH^- doped alkali halides and also through the observation of an

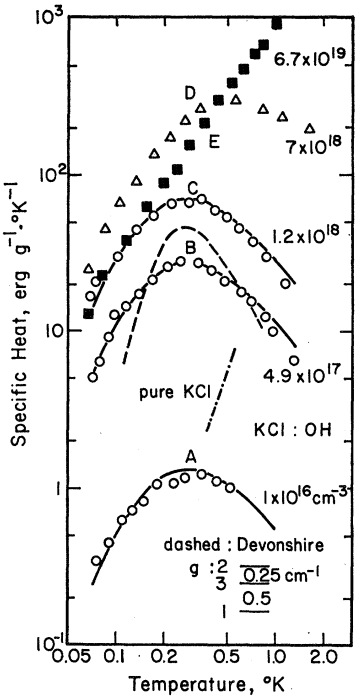

FIG. 31. Excess specific heat of KCl:OH (PHP69). For concentrations up to 1.2×10^{18} cm^{-3}, the shape of the anomaly is concentration independent; the same solid curve, shifted vertically, fits the curves A, B, and C. A Schottky anomaly computed for a three-level system with splittings close to those derived from paraelectric resonance work, see Bron and Dreyfus (BD67), fits the data reasonably well, as shown by the dashed curve. The specific-heat anomaly computed using Scott and Flygare's value of the tunnel splitting, see Fig. 32, has a shape similar to the Devonshire anomaly, but is shifted to lower temperatures (R. L. Pompi, private communication).

electrocaloric effect (KL65, SF65). These measurements further showed that the OH^- ion has six equilibrium orientations pointing along the six ⟨100⟩ crystallographic directions. In measurements of the ac dielectric constant between 10^2 and 10^4 cps above 0.3°K, Känzig *et al.* (KHR64) showed that OH^- in KCl is highly polarizable and estimated the tunnel splitting to be smaller than 0.2 cm^{-1} (0.3°K).

Thermal conductivity measurements by Chau *et al.* (CKW67) and by Rosenbaum (Ro68, RCK69) indicated resonance scattering below 0.3°K in KCl:OH, the lowest temperature of their measurements, and at 0.5°K in NaCl:OH. From this, Rosenbaum determinated a tunnel splitting of approximately 0.4 cm^{-1} for KCl:OH and of 1.5 cm^{-1} for NaCl:OH.

The first direct evidence for the tunneling states of the OH^- ion was obtained from measurements of paraelectric resonance. The spectra obtained in KCl:OH with microwaves of frequency 9 GHz (BD66), 24.6 GHz (SE66), and 35.2 GHz (FSS66) were explained on the basis of the Devonshire potential in the high barrier limit (tunneling between localized librational states). The tunnel splitting between the lowest and the first excited state (A_{1g}–T_{1u}) was determined to be 0.4 cm^{-1}, and between the second and the third (T_{1u}–E_g), to be 0.2 cm^{-1} (BD67, Dr69). Because of the very strong microwave absorption by OH^- ions, OH^- concentrations as they are usually found in undoped crystals ($n_{OH}\approx10^{16}$ cm^{-3}) had been used for most of these resonance experiments, and the scaling between the resonance spectrum and the OH^- concentration had not been studied with sufficient care. It was later shown by Höcherl *et al.* (HBW67) that of the two lines observed at 35 GHz (FSS66) in KCl:OH, the one at low field (7.1 kV/cm for $E \parallel [100]$) was probably caused by an impurity other than OH^-, which they have since identified (HW68) as Li^+. This observation has cast some doubt on the interpretation of the earlier resonance work; Estle (Es68) for instance, concluded that part of the OH^- spectra was probably caused by a defect with equilibrium orientations along ⟨111⟩, such as Li^+.

Härtel and Lüty (HL68) have recently studied the electric field induced dichroism of the OH^- stretching vibration using very high resolution ($\approx$0.1 cm^{-1}). At $T=5$°K, they observed only one narrow (half-width $\tilde{\Gamma}=0.13$ cm^{-1}) absorption line. For a tunnel splitting of the magnitude derived from the paraelectric resonance work, the absorption should consist of several lines, corresponding to an excitation of the stretching vibration plus (or minus) the tunneling energies, see Chapter V.A. For the lowest two tunneling states, this would result in two lines 0.8 cm^{-1} apart, in contrast to the experimental finding of the single, narrow line. Obviously, one possible explanation is that the tunnel splitting is indeed smaller, with the upper limit of the splitting given by the half-width of the experimental absorption line (0.13 cm^{-1}). The same conclusion was reached by Dick (Di68): From the relaxation time of the OH^- ion in KCl determined from dielectric (BDK65) and electrocaloric (Lu67) measurements and from its stress dipole moment (HL65, Ha66), he derived a tunnel splitting for OH^- in KCl about 10 times smaller than that deduced from the resonance work.

Recently, a specific-heat anomaly in KCl:OH has been observed by Peressini *et al.* (PHP69), see Fig. 31. Its entropy is given by $n_{OH}k_B \ln 6$, where n_{OH} is the OH^- concentration determined from the optical absorption (KKGW68). Hence the motional ground state consists of six states, in agreement with potential minima in the six ⟨100⟩ directions. Up to $n_{OH}=1.2\times10^{18}$ cm^{-3}, the shape of the anomaly is independent of concentration. This rules out cooperative phenomena as a source of the anomaly. (The higher-concentration data will be considered in VI.B). A Schottky specific-heat anomaly based on a Devonshire potential provides a satisfactory description of the anomaly, with a tunnel splitting of 0.5 cm^{-1} between A_{1g} and T_{1u}, and of 0.25 cm^{-1} between T_{1u} and E_g, close to the splittings derived from the paraelectric resonance.

The specific-heat measurements strongly support the tunneling model. The single, narrow absorption line observed for the stretching vibration (HL68) of OH^-,

however, still poses a very serious question. Perhaps, random internal stresses and electric fields cause a violation of the usual parity selection rules.

The tunneling states of KCl:OH and NaCl:OH have also been studied by microwave absorption at zero field between 8 and 40 GHz (Sc69, SF69). The absorption bands were explained in the framework of the Devonshire potential with an additional perturbing potential of symmetry C_{4v}, as caused, for instance, by a uniform (local) electric field of 6.5 kV/cm (in KCl). As the origin of such a perturbation Scott and Flygare assumed that the center of mass of the OH^- ion does not coincide with the cavity center, but is displaced in a [100] direction. This model is similar to that proposed by Shore (Sh66a) and by Pompi and Narayanamurti (PN68) except that their perturbing potential had tetragonal symmetry, corresponding to an elastic distortion of the cavity potential in a [100] direction. Figure 32 shows the OH^- tunneling energies in the Devonshire model, and also the influence of an applied electric field. The internal perturbing field, according to Scott and Flygare (Sc69, SF69), is also indicated. According to their analysis, the splitting between the lowest two states is 0.38 cm^{-1} (11.5 GHz, 0.28×10^{-4} eV). The splitting obtained by fitting an exponential curve to the low-temperature side of the specific-heat anomaly is 0.3 $cm^{-1}\pm10\%$.

In NaCl:OH (Sc69, SF69) the tunnel splitting appears to be larger than in KCl:OH. This agrees with the thermal conductivity results (Ro68, RCK69), from which a resonance frequency of 1.5 cm^{-1} was obtained, and with a recent study of the far-infrared librational absorption by Kirby *et al.* (KHS68) in which evidence for a tunnel splitting of 2 cm^{-1} was reported.

In nominally pure NaF, specific-heat measurements by Harrison *et al.* (HLP68) have given evidence for tunneling states, which they ascribed to OH^-. With a Devonshire model, the anomaly can be fitted with the splitting of 0.4 cm^{-1} (A_{1g}–T_{1u}) and 0.2 cm^{-1} (T_{1u}–E_g).

Resonance scattering in LiF containing OH^- has also been observed (Th65). The resonance frequency is approximately 1.8 cm^{-1}. The data will be shown later, Fig. 34.

Because of the success of the Devonshire model in describing not only the tunneling states, but also the librational and rotational states of the CN^- ion in solid solution, this model has also been applied to the higher excited motional states of the OH^- ion. On the whole, however, the agreement has been poor, as has been discussed by Klein and co-workers (WK69, KWL69). It is, therefore, somewhat surprising that the tunneling states of the OH^- ion appear to agree reasonably well with this model. Among the possible reasons we mention that a distortion of the potential may influence the states near the top of the potential barrier more than the ones near the bottom of the wells. Furthermore, we must recall a very important simplifying assumption

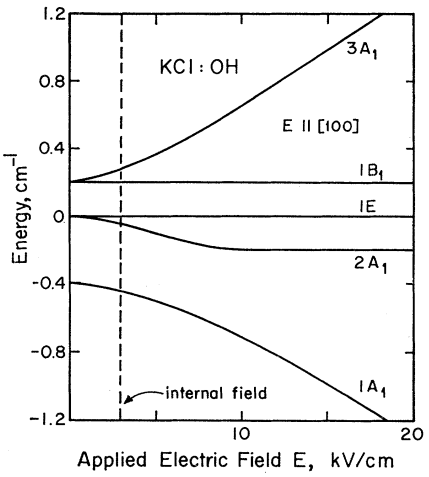

FIG. 32. Tunneling states of KCl:OH according to the Devonshire model ($E=0$) and in an electric field applied parallel to a [100] crystallographic direction. The microwave absorption experiments by Scott and Flygare (SF69) have given evidence that the OH^- ion in KCl is moving in a potential containing in addition to the Devonshire potential one of symmetry C_{4v} which can be viewed as a local electric field $E=6.5$ kV/cm. The dashed line indicates the corresponding applied field of 3 kV/cm. This internal field is suggested to result from a displacement of the OH^- ion from the cavity center.

made by the Devonshire model, namely that of a stationary potential in which only the impurity ion moves. This assumption appears justified for motional states of low frequencies, as was seen in the cases of CN^- and Li^+. In the case of OH^-, however, where librational frequencies near the host's Debye frequency have been observed, the coupling may become too large to permit a separation of the motion of the impurity ion from that of the surrounding lattice. The question of the frequency dependence of the coupling between the motional states of the defect and the lattice will be considered again in Chapter VI.A.

E. Other Possible Cases of Tunneling

In the four preceding sections, all those cases in which the existence of tunneling states is firmly established have been described. In this section, those impurities for which indirect evidence of tunneling states exists, as well as of those for which tunneling can be safely discounted, will be reviewed.

The NO_2^- ion is an asymmetric top which has three infrared-active normal modes and three axes of rotation, shown in Fig. 33. From a study of the fine structure of these modes in the near infrared as a function of temperature, Narayanamurti *et al.* (NSP66) concluded that this ion must have several low-lying tunneling states in the potassium halides, connected with rotational motions around its three axes. The most detailed picture was obtained for KCl, where the tunnel splitting for rotation around the A axis was found to be 2 cm^{-1}. The splitting for tunneling around the B axis was estimated to be 0.002 cm^{-1}, and around the C axis,

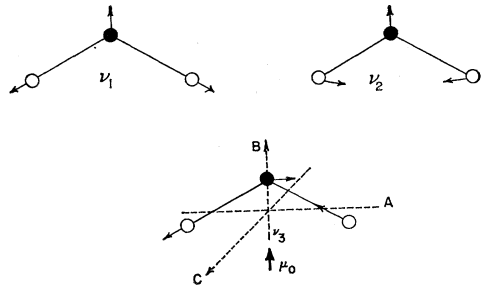

FIG. 33. Normal modes of vibration of the NO_2^- molecule. The three principal axes of rotation and the direction of the permanent dipole moment μ_0 are indicated (NSP66).

<0.5 cm^{-1}. Thermal conductivity measurements gave evidence for a tunnel splitting of 0.8 cm^{-1} or less. In measurements of the dielectric constant (SM65) of KCl:NO_2 above 2.5°K, a $1/T$ dependence was found, indicating a ground-state splitting of less than 2 cm^{-1}.

In KBr and KI, evidence for tunneling of the NO_2^- ion around the A and B axes, respectively, was found; but, because of simultaneous evidence for a displacement of the center of mass of the ion in its cavity, the picture appeared to be more complicated than in KCl.

That NO_2^- in NaCl, and NO_3^- in NaCl, KCl, KBr, and KI are immobile at low temperatures was demonstrated through the lack of low-temperature stress induced infrared dichroism (NSP66).

The ammonium ion, NH_4^+, substituting for the alkali ion in alkali halides, was found by means of ir spectroscopy to perform hindered rotations at low temperatures (VH61, Ki60). Some of the low-lying levels may be due to tunneling. Evidence for the presence of low-lying motional states which are strongly coupled to the phonons has also been obtained from thermal conductivity measurements by Seward, who found that a KBr crystal into which approximately 10^{18} cm^{-3} NH_4^- ions had been diffused had a conductivity reduced by a factor of 10 in the temperature region from 1 to 6°K, in a way similar to KBr containing NO_2^- ions (NSP66, Po63). The energies of these scattering centers are of the order of a few wavenumbers.

The ions SH^- and SeH^- can also substitute for halogen ions in alkali halides (FG65, FJ67). SH^- in KBr is believed to have tunneling states which were detected in paraelectric resonance (BD66). In KCl:SH no tunneling states were found. On SeH^- no measurements are available.

The observation of an electrocaloric effect (LP66, RP69) in NaBr:F at temperatures as low as 0.3°K has established a high mobility of the F^- ion in the Br^- vacancy, with a dipole moment $p_0 \approx 4$ D (uncorrected for local field). The value quoted here is larger than the one given in (RP69) due to an error in the concentration in the earlier work (Ro69). Thermal conductivity measurements, however, have failed to show the strong phonon resonance scattering which was observed with all defects known to tunnel. A specific-heat anomaly has been found in NaBr:F, which scales with the F^- concentration and whose entropy is close to $nk_B \ln 6$, but whose shape differs greatly from a Schottky anomaly (LP66, RP69). Instead it varies almost linearly with temperature from 0.05°K up. One of the possible explanations of this shape is that random internal strains cause the potential minima of the off-center F^- ion to be very unequal, in a way comparable to the O_2^- ion in alkali halides (Si69), see Chapter IV and Fig. 6. In this case, the specific heat would detect the thermal repopulation among the different potential minima, and not the tunneling frequencies. A detailed study of this problem is currently in progress (Ro69).

Electric cooling has also been observed in RbCl:Ag (KL68), and a dipole moment $p_0 = 4.0$ D has been determined. In the high-field limit, cooling was larger for the electric field E applied $\parallel$ [111] than for $E \parallel$ [100], similar to the findings in KCl:Li. This suggests that the Ag^+ ion has eight potential minima along the eight ⟨111⟩ cube diagonals. A central instability of the Ag^+ ion in RbCl has been predicted earlier from measurements of the temperature dependence of the oscillator strength observed for the ultraviolet Ag^+ absorption (DF66), with a barrier height for motion through the cavity center of approximately 100 cm^{-1}. Details of the motional ground state of the Ag^+ ion are not known, but tunneling seems likely. Specific-heat measurements are in progress (Ro69).

The absence of an electrocaloric effect in the cases of monatomic defects and of molecules with a permanent dipole moment is an indication that tunneling is negligible in the librational ground state. This is the case in the following substances: KCl doped with Ag^+ or Rb^+ (LP65), with F^- or Cu^+ (Ro69), F centers (LP65); KBr doped with Li^+ (LP66, RP69), H^- (LP65), or Cu^+ (Ro69); RbCl doped with Li^+, F^-, or Cu^+ (Ro69), or Na^+ (Lo70); and RbBr doped with Ag^+ (KL68).

Specific-heat measurements on KBr:Li showed no evidence for any low-lying states between 0.01 and 10 cm^{-1} (HPP68a). This agrees with the findings in elastic (BS68) and far-infrared optical (NS66, NS68) measurements, which lead to the conclusion that the equilibrium location of the Li^+ ion in KBr is at the cubic site. A negative result was also obtained by Huiskamp and co-workers on NaBr:Li (Hu69): No excess specific heat above 0.1°K was observed on one sample which had an estimated Li^+ concentration of 10^{18} cm^{-3}.

F. Summary

The investigations reviewed in this chapter have demonstrated that ions in solids can tunnel with remarkably high frequency, and have also provided a rather detailed picture of the tunneling states themselves. Two different types of tunneling have been

observed: tunneling connected with a rotational motion, for which the CN^- ion in KCl is a good example, and tunneling connected with a translational center-of-mass motion, as found in KCl:Li. In spite of the different nature of the rotational and the translational tunneling, the tunneling states themselves have been described successfully with the same model, namely a dumbbell whose rotational states are perturbed by the stationary crystal field. In the simplest cases, as in KCl:CN and KCl:Li this field has the same symmetry as the lattice, whereas in the more complicated cases, as in RbCl:CN or KCl:OH the crystal field is probably somewhat modified.

Internal stresses σ_i of the order of 100 N cm^{-2} (10 atm) appear to be typical in alkali halide crystals. The elastic dipole moments p_λ of the tunneling defects are of the order of 10^{-23} cm^3, and hence the perturbation energies of the tunneling states resulting from these stresses are $\sigma_i p_\lambda \approx 10^{-4}$ eV, or of order 1 cm^{-1}. Hence, it is to be expected that for defects with tunneling frequencies less than 3×10^{10} sec^{-1} (1 cm^{-1}) the motional states will be determined to a large extent by the internal stresses. The O_2^- ion, which has a very small tunneling frequency (about 10^{-6} cm^{-1}) appears to be a prime example of the dominating influence of the internal stress which can, therefore, be studied using this ion. In the other extreme, for defects with large tunnel splitting, as for CN^- or Li^+ in KCl, the perturbation by σ_i is relatively weak. Finally, there may be intermediate cases, like KCl:OH, RbCl:CN, and NaBr:F, where the influence of σ_i becomes increasingly more important.

Calculations of the lattice energy in the case of off-center ions have shown that the ions around the impurity move from their original lattice sites by amounts comparable to the displacement of the impurity ion itself (WHDS67). Yet the experimental evidence speaks against a participation of the host ions in the motion of the impurity. For example, the isotope effect in KCl:Li can be quantitatively explained in the framework of a rigid potential of cubic symmetry. If the six, heavy nearest-neighbor Cl^- ions were allowed to move by the amounts predicted theoretically, the predicted isotope effect would be far too small. This conclusion is the same as that reached by Kirby *et al.* (KNAS68) regarding the isotope effect in the case of lattice resonant modes. The reason why the inclusion of the motion of the neighboring ions in the dynamics of the in-band impurity modes has been without success is presently not understood.

For a listing of some of the pertinent data concerning the tunneling states we refer to Fig. 37 in VI.A and Table I in VI.D.

VI. SOME APPLICATION OF TUNNELING STATES

Tunneling states with an electric polarizability are the electric analogs to spin states of magnetic impurities, and therefore offer themselves for a wide variety of studies which are analogous to the studies so far restricted to their magnetic counterparts. In this chapter we want to review some of the electric analogs of spin–phonon, spin–spin, and spin–photon interaction. We begin with the study of the interaction between tunneling states and phonons.

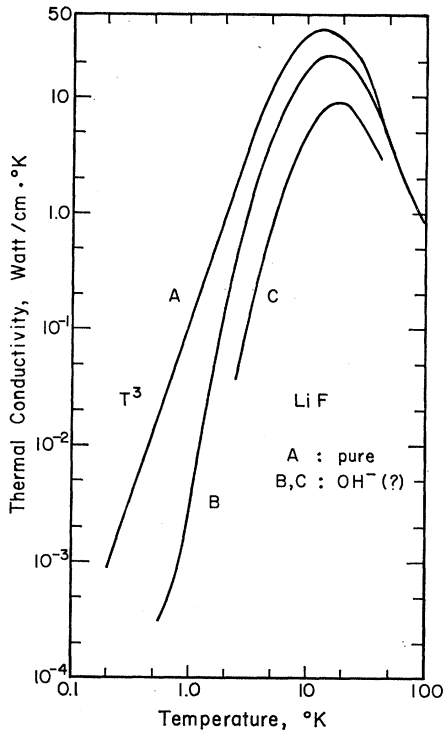

FIG. 34. Thermal conductivity of LiF. Curve A: pure. The thermal conductivity of pure LiF has been measured to 0.05°K and has been found to vary as T^3 even at these temperatures [Harrison (Ha68)]. Curve B: unintentional OH^- impurity, absorption constant of ultraviolet absorption band at 10 eV: $\alpha_{OH} = 0.6$ cm^{-1} (Th65). Curve C: this crystal of isotopically pure ^{6}LiF, prepared by Sproull in an attempt to study the influence of isotopic mixtures on the thermal conductivity, is believed to contain OH^- ions resulting from the wet chemical preparation of the starting material. Estimated OH^- concentration in the range of 10^{17}–10^{18} cm^{-3}. The position of the dip (0.65°K) in the thermal conductivity curve indicates a resonance frequency $\tilde{\omega}_0 \approx 1.8$ cm^{-1} (3.4×10^{11} rad/sec).

A. Coupling of the Tunneling States to the Lattice

All crystals containing impurities with tunneling states have greatly reduced thermal conductivities, see Figs. 8, 16, and 21. Figure 34 shows what is now believed to be the first observation of such a scattering. In nominally pure LiF, Sproull observed an anomalously low thermal conductivity which varied as the fourth or fifth power of temperature at the lowest temperatures studied (Sp57). Carruthers suggested that such a strong temperature dependence could result from a phonon resonance scattering process, i.e., scattering by discrete energy states (Ca62). By extending the measurements below 1°K, Thacher demonstrated the

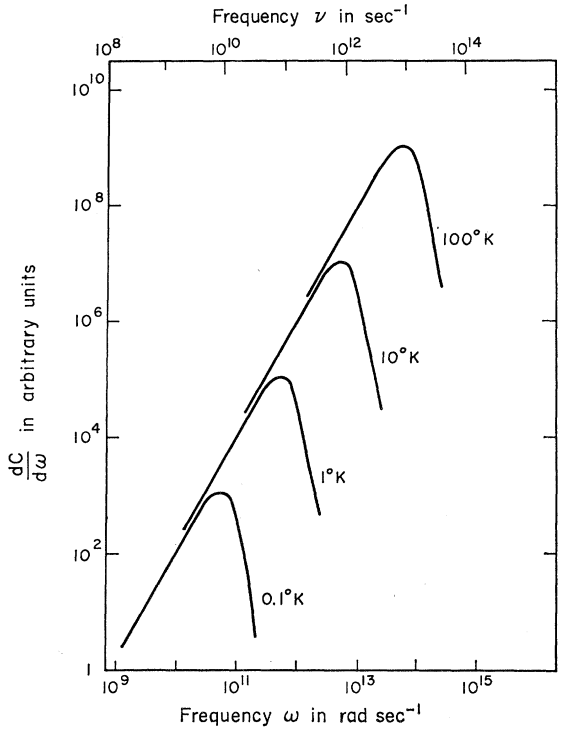

FIG. 35. The contribution of the phonon angular frequency interval $d\omega$ to the lattice specific heat in the Debye approximation for four different temperatures (Po69). The frequency ω_{dom} at the maximum of the curves shifts towards higher phonon frequencies in linear proportion with T: $\omega_{dom}=5.65\times10^{11}$ rad/sec $T(°K^{-1})$ or $\tilde{\omega}_{dom}=3$ cm^{-1} $T(°K)^{-1}$.

resonance dip in the thermal conductivity curve (Fig. 34) and found that the scattering scaled with an optical absorption in the ultraviolet at 10 eV caused by OH^- ions (Th65). It is believed that this scattering is caused by resonance interaction of phonons with the tunneling states of these impurities.

We now turn to the problem of extracting quantitative information about the resonance scattering process from thermal conductivity measurements. In the first approximation, the thermal conductivity can be written in the form of Eq. (16). Thus an average phonon defect scattering rate $\bar{\tau}_{def}^{-1}(T)$ can be obtained as was done in Chapter V.C and Fig. 22. Since, at any given temperature, the heat will be carried predominantly by phonons of a certain frequency range ω_{dom}, this method can even be used for a crude determination of a frequency-dependent scattering rate $\bar{\tau}_{def}^{-1}$ (ω_{dom}). For details, see caption of Fig. 22.

A more precise method for the analysis of thermal conductivity data begins with the assumption of a Debye phonon spectrum in the crystal. The conductivity can then be expressed as an integral over the Debye density of states:

$$K=\tfrac{1}{3}\int(dC/d\omega)v^2\tau\,d\omega, \qquad (32)$$

where τ is a relaxation time which is a function of frequency and perhaps also of temperature. The use of a relaxation time implies that if different scattering processes are active, the total relaxation time is given by

$$\tau^{-1}=\sum_i \tau_i^{-1}, \qquad (33)$$

where τ_i describes the individual scattering process. This so-called Debye model of thermal conductivity employs essentially two important simplifying assumptions: First, by using the Debye density of states, the model ignores all modal or directional dependencies. The phonons and their scattering are characterized by the phonon frequency ω alone. The quantity $dC/d\omega$ is shown in Fig. 35. The second and more profound assumption is the single mode relaxation time itself, together with the implicit assumption of a local temperature in the crystal. The validity and limitations of the Debye model have been investigated both theoretically and experimentally (Ca59, Po69). The Debye model has been used rather extensively for the description of phonon resonance scattering in thermal conductivity. The results will be reviewed in the following.

In crystals containing impurities with tunneling states, a defect relaxation rate $\tau_{def}^{-1}(\omega)$ of the following form has been very successful in describing the addi-

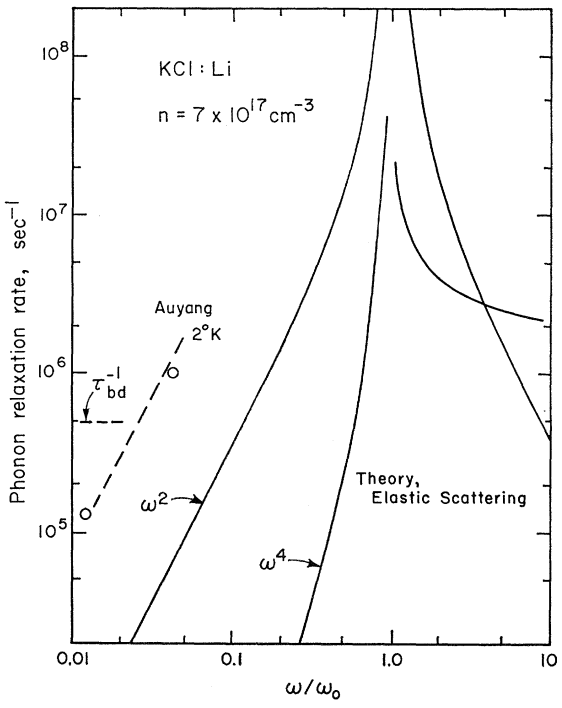

FIG. 36. The phenomenological relaxation rate τ_{def}^{-1}, Eq. (34) used to obtain a best fit to the thermal conductivity of KCl:^{7}Li, $n_{Li}=7\times10^{17}$ cm^{-3} (Ba64, BHPS67). Also shown is the relaxation rate calculated for phonon resonance fluorescence scattering by a classical stress dipole, see later, Eq. (35). Apart from the wrong frequency dependence at $\omega/\omega_0\ll1$, the agreement between the two relaxation rates is reasonable. Also noted are the relaxation rates determined through ultrasonic attenuation by Auyang (Au68) for longitudinal [111] waves at 2°K. For longitudinal [100] waves, no attenuation was observed.

tional phonon scattering:

$$\tau_{\text{def}}^{-1}(\omega) = nA[\omega^2/(\omega_0^2-\omega^2)^2]. \quad (34)$$

Here n is the defect concentration determined chemically; the resonance frequency ω_0 and the so-called scattering strength A are adjustable parameters.

Figure 36 shows the relaxation rate τ_{def}^{-1}, as given by Eq. (34), used to obtain a best fit to the conductivity of KCl:Li. Examples of the quality of the fits can be found in Figs. 8, 16, and 21. Both A and ω_0 were found to be concentration independent over several orders of magnitude in concentration except at very high concentrations in KCl:Li (PHP69) and in KCl:OH (Ro68, RCK69), where saturation of τ_{def}^{-1} was observed (see VI.b).

In the context of this paper, only the resonances at the lowest temperatures are important, but resonances at higher temperatures, which are believed to result from scattering by higher rotational states or by resonant modes of the lattice, have also been well

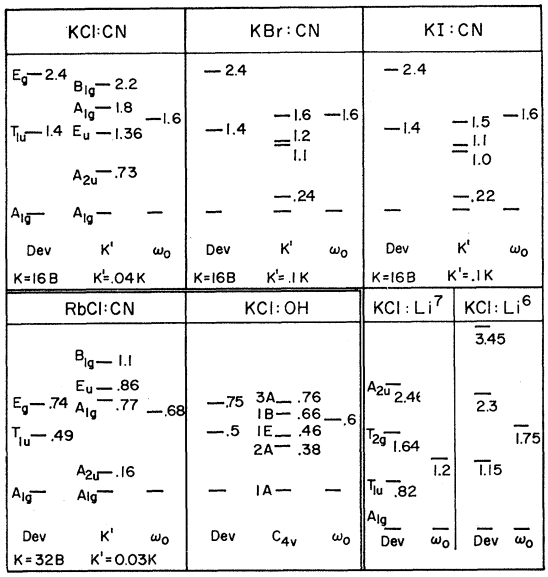

FIG. 37. Comparison of the energies of the tunneling states for CN^-, OH^-, and Li^+. All energies measured in wavenumbers above the ground state. Scales for RbCl:CN and KCl:OH are twice as large as those of the rest. It means: Dev, energies determined from near-infrared absorption and/or specific-heat measurements, using the Devonshire potential. K', distorted Devonshire potential, see Chapter V.B. ω_0 is the resonance frequency from thermal conductivity. Note that in NaCl:CN, for which no tunnel splitting was observed in the infrared work, no low-temperature resonant scattering was found. CN^-: see SN66 and HPP68 for Dev and ω_0; PPHN69 and PN68 for K'. KCl:OH: the values labeled Dev were obtained from best fit to specific heat (PHP69a), using Devonshire potential in high barrier limit; from paraelectric resonance the values are 0.4 and 0.6 cm^{-1}, respectively (BD67); the values labeled C_{4v} were deduced from microwave absorption experiments, (Sc69, SF69); from low-temperature specific-heat measurements (PHP69a), the splitting between the lowest two tunneling states was determined to 0.33 $cm^{-1}\pm10\%$. The resonance frequency ω_0 obtained from thermal conductivity is uncertain since measurements do not extend to sufficiently low temperatures. Rosenbaum fitted his data with a resonance frequency of 0.4 cm^{-1}.

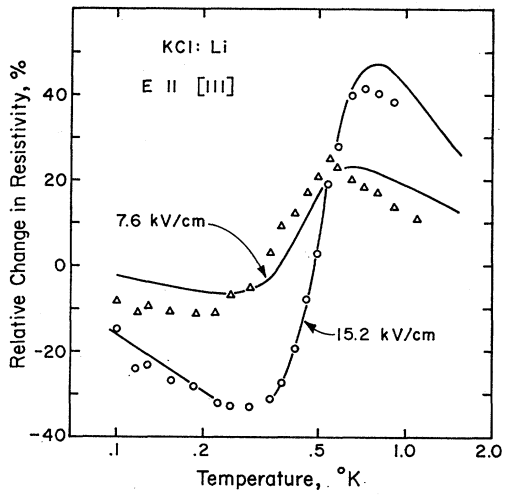

FIG. 38. Relative change of thermal resistivity (reciprocal conductivity) for electric field applied parallel to [111] and perpendicular to the heat flow (which was in [112]) for two different electric fields. $n=1.6\times10^{17}$ cm^{-3} (10 ppm). The solid curves were computed from the least-squares fits to the experimental thermal-conductivity curves (PHP69).

described using Eq. (34), provided they do not occur in the temperature region where phonon–phonon scattering becomes important in the host crystal (Po62, VH61, HPP68); an example of such a fit is contained in Fig. 8, where the dip at 6°K is ascribed to the onset of free rotation of the CN^- ion. See also KSV69.

A comparison of the resonance frequencies ω_0 producing best fits to the conductivity curves with the tunnel splittings determined from infrared and microwave spectroscopic and from specific-heat measurements, see Fig. 37, shows the close connection between the tunneling states and the resonance frequency. The fact that in KCl:Li the isotope effect of ω_0 (45%) (PHP69) is practically identical to that observed for the tunnel splitting Δ_0 (40%) (HPP68a, He68, HS69, SS69, Sh69) demonstrates that the scattering indeed results from an interaction with the tunneling states themselves. The tunneling states of KCl:Li were also split in an electric field applied to the crystal perpendicular to the heat flow. Figure 38 shows the results. In an electric field, the scattering by the lithium ions is also described by the relaxation rate, Eq. (33); ω_0, as determined by a best fit to the data, increases in the electric field in almost the same way as the average tunneling splitting increases, see the open circles in Fig. 39. These observations suggest that the phenomenological relaxation rate of Eq. (33) comprises the resonance scattering by the several tunneling states, and that ω_0 is some average of the tunneling frequencies.

Direct evidence for phonon resonance scattering by the individual tunneling states was obtained by Walton (Wa67). His experiment is explained with the help of Fig. 40, top: The integrand $dK/d\omega$ of the thermal conductivity integral $K(T)$ is plotted as a function of ω. The phonons of energy Δ_0, $2\Delta_0$, and $3\Delta_0$ are assumed

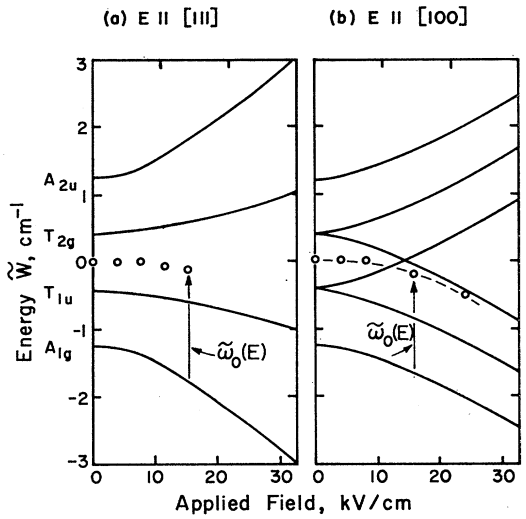

FIG. 39. KCl:Li. Stark effect of ^{7}Li tunneling states, comparison with the resonance frequencies $\omega_0(E)$ determined from thermal conductivity. At the temperature of measurement, most ions are in their ground state, and phonon induced transitions will, therefore, go from this state to the excited tunneling states. Open circles: ω_0 determined with single resonance expression [Eq. (34)] (PHP69).

to be scattered strongly by the lithium tunneling states. In addition to the lithium ions, the crystal contains a spin system which resonantly interacts with the phonons, and whose resonance frequency ω_s can be tuned with a magnetic field B. If ω_s lies in a frequency region in which the phonons are relatively little scattered by the tunneling states, i.e., where $dK/d\omega$ of KCl:Li has maxima, the spin system will reduce the conductivity more than if ω_s equals one of the tunneling frequencies. As magnetic defects, Walton used color centers produced by optically bleaching F centers in the KCl:Li crystals. These defects are probably R centers, which have spin 1/2 and which are strongly coupled to elastic strains as demonstrated by stress induced dichroism (Si65). Figure 40, bottom, shows three distinct minima of the relative change in conductivity $|\Delta K/K_0|$ at 7, 14, and 23 kG. For a g value of 2, this corresponds to resonance energies of 0.7, 1.4, and 2.3 cm^{-1}, as compared to the tunneling splittings 0.82, 1.64, and 2.46 cm^{-1} for KCl:^{7}Li, see Fig. 39. In KCl:CN, two minima of $|\Delta K/K_0|$ were found with the same technique (HW69), corresponding to the A_{1g}–T_{1u} and the A_{1g}–E_g transitions for the CN^- ion (Fig. 37). From the shape and depth of the minima, it should be possible to determine the scattering strength of the individual transition, once the magnetic defect is better understood. In his work, Walton noticed that the relative depths of the minima were strongly sample dependent, which he suggested to be caused by internal strains. Nevertheless, it appears that the phonons do indeed couple to all tunneling states with about equal strength. It is remarkable that the even–even and odd–odd transitions do not appear much stronger than the even–odd transitions as one would expect in the case of coupling of the elastic dipole with the phonon stress. Conceivably, internal stress or electric fields (He68, HS69) change the symmetries of the tunneling states and thus alter the selection rules for the phonon scattering.

For a crude but fairly successful description of the phonon scattering by the tunneling states, the defect is approximated by a classical elastic dipole embedded in an elastic continuum. Such a dipole will scatter an elastic wave by resonance fluorescence with the following relaxation rate (Po68):

$$\tau_{\text{def}}^{-1}=n4\pi v^3\alpha^2\omega^4/[(\omega_0^2-\omega^2)^2+(\alpha\omega^2)^2\omega^2], \quad (35)$$

where n is the number density of the scattering centers, v the velocity of sound, and ω_0 the resonance frequency of the scatterer. $(\alpha\omega^2)^{-1}$ is the time during which the oscillator loses 63% of its energy W by radiation,

$$W=W_0\exp(-\alpha\omega^2 t). \quad (36)$$

For an elastic dipole of moment p_λ, rotational inertia I, performing angular motion $\theta(t)$ in a medium of stiffness C_s, α is given by (Po68)

$$\alpha=2p_\lambda^2/3(4\pi C_s)^{-1}v^3 I. \quad (37)$$

In the Debye approximation, v and C_s are connected by

$$v=(C_s/\rho)^{1/2}, \quad (38)$$

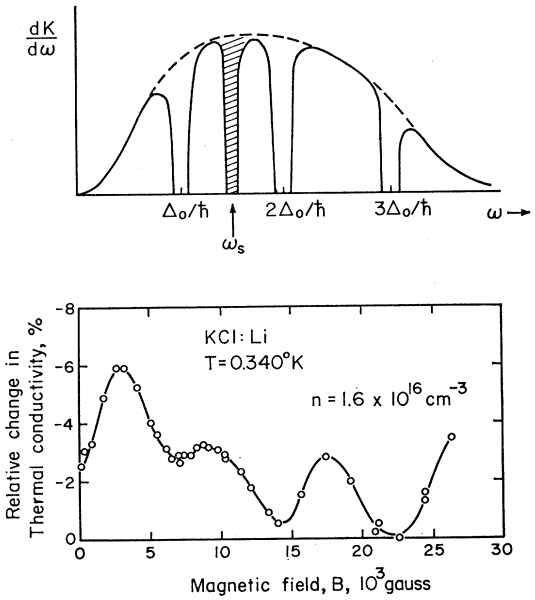

FIG. 40. Top: integrand $dK/d\omega$ of the thermal conductivity integral, as a function of phonon frequency ω. The three depressions are caused by resonance scattering off the lithium tunneling states. An additional magnetic impurity can also cause a certain frequency band to be removed from $dK/d\omega$ (see the crosshatched area). Bottom: observed relative change of the conductivity, $\Delta K/K_0$, as the magnetic impurity is tuned with an external B field. Normal isotopic mixture (92.6% ^{7}Li, 7.4% ^{6}Li). At 0.34°K, practically all Li^+ ions are in the lowest tunneling state. The shape of the curve varies from sample to sample. In one instance, the 7-kG minimum appeared much stronger, and the 14 kG one, weaker than shown here. After Walton (Wa67).

where ρ is the mass density of the host. For Li^+ and CN^- all quantities entering in Eqs. (35)–(38) are known; ω_0 is taken from the thermal conductivity fit, and p_Λ is obtained from elastic measurements, see Table I in Chapter VI.D. The rotational inertia in the case of the Li^+ ion is taken as $I=mr_0^2$, where m is the mass of the Li^+ ion, and r_0 the distance of the potential minima from the cavity center, $r_0=1.2$ Å [Eq. (30)]. Figure 36 shows the comparison of the theoretical relaxation rate with the experimental one. In spite of the crudeness of the model, theory and experiment agree within an order of magnitude. A serious discrepancy is found only at low frequencies, where the experimental scattering drops off as ω^2 [Eq. (34)] rather than as ω^4 [Eq. (35)] (Po68).

The empirical scattering strength A of Eq. (33) has been compared for several impurities and hosts. Figure 41 shows a surprisingly simple result (Po68): In the first approximation, A is independent of the defect and its host and is proportional to ω_0^2:

$$A=c\omega_0^2,\ c\approx 10^2(\mathrm{cm}^3/\mathrm{sec}^3)\,(\mathrm{sec/rad})^{-2}. \qquad (39)$$

It is of particular importance that this relation was also found to hold when ω_0 was changed by an electric field applied to the crystal (PHP69).

A phenomenological model has been proposed (Po68) to explain both the low-frequency ω^2 dependence of $\tau^{-1}(\omega)$ [Eq. (34)] and the relation Eq. (39), in which it was assumed that the oscillators lose their energy through a viscous (i.e., not frequency dependent) damping whose magnitude is equal to that of the oscillators radiating at resonance frequency ω_0:

$$W=W_0\exp(-\alpha\omega_0^2 t). \qquad (40)$$

The average life times of the excited tunneling states derived with the help of this model are listed in Table I shown in VI.D. They agree with those determined with other techniques. A detailed picture for the coupling to the lattice is still missing.

It should be mentioned at this point that the dielectric measurements by Känzig and co-workers (BDK65, KKP67) on KCl:OH and KBr:OH indicated that the relaxation rate of the dipolar reorientation increased linearly with temperature up to 10°K. This supports the picture of a one-phonon process, an assumption tacitly made throughout the preceeding discussion.

The thermal conductivity measurements described above have shown that the phonon resonance scattering is caused by an interaction with the tunneling states. In order to understand the details of the interaction process, experimental techniques with higher resolution are needed. Byer and Sack (BS68) and Auyang (Au68) studied the attenuation of ultrasound in the angular frequency range from $\omega=2\pi\times3\times10^7$ sec^{-1} to $\omega=2\pi\times1.745\times10^9$ sec^{-1} in KCl:Li above 2°K. For transverse sound propagating in [110], polarized in [001] (BS68), and for longitudinal sound propagating in [111] (Au68), they observed an increase of the attenuation

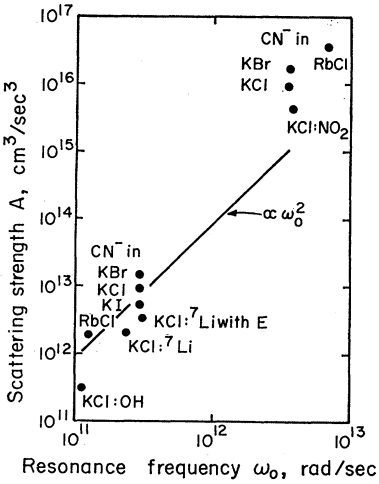

FIG. 41. The quantity A from Eq. (34), as determined by a best fit to thermal conductivity data for scattering by tunneling and rotational states (Po68). For KCl:OH, A was estimated from the measurements by Chau *et al.* (CKW67) and by Rosenbaum (Ro68, RCK69) by comparing $\bar{\tau}^{-1}$ [see Eq. (17)] with that of other crystals containing tunneling states.

which scaled with the lithium concentration and which varied as ω^n/T, with $n\approx2$. For transverse sound propagating in [110], polarized in [1$\bar{1}$0] (BS68), and for longitudinal sound propagating in [100] (Au68), no lithium induced attenuation was observed. In these cases, the attenuation was at least 100 times less than in the cases in which attenuation was observed. This selectivity of the attenuation was explained with the model of a classical stress dipole with equilibrium orientations along the eight ⟨111⟩ directions which can line up in a stress field (NH65). Certain stresses lower the energy of some of the eight potential minima and cause the population of these wells to increase. The stresses associated with the trigonal (T_{2g}) [110] transverse sound, polarized in [001], and the longitudinal [111] sound will do just this, whereas the stresses associated with the other, tetragonal, sound waves do not cause an alignment of the dipoles.

The alignment is a dissipative process, and hence the attenuation of the ultrasonic energy has been viewed by Byer and Sack (BS68) as a Debye relaxation process, resulting in the reciprocal lifetime, τ_{us}^{-1}, of the ultrasonic energy:

$$\tau_{us}^{-1}=(\Delta S/S)[\omega^2\tau_{orient}/(1+\omega^2\tau_{orient}^2)], \qquad (41)$$

where $\Delta S/S$ is the relative change of the elastic compliance S resulting from the alignment, and τ_{orient} is the time in which the dipoles follow the stress field. For trigonal stress, elastic dipole theory shows

$$\Delta S(T_{2g})=\Delta S_{44}=4n_{Li}p_\Lambda^2/9k_BT, \qquad (42)$$

hence

$$\tau_{us}^{-1}=(4n_{Li}p_\Lambda^2/9k_BTS)[\omega^2\tau_{orient}/(1+\omega^2\tau_{orient})], \qquad (43)$$

which varies as ω^2/T if $\omega^2\tau_{\text{orient}}<1$, in agreement with the experiment. The dipole reorientation time τ_{orient}, determined from the measured ultrasonic attenuation by using Eq. (43), however, was found to be between 10^{-10} and 10^{-11} sec, i.e., of the same order of magnitude as the tunneling frequency, and about two orders of magnitude smaller than the dipole–lattice relaxation time determined from other experiments (see below, Table I). In addition, a comparison of the ultrasonic attenuation rate τ_{us}^{-1} for longitudinal [111] sound (Au68) with the phonon attenuation rate τ^{-1} derived from thermal conductivity, Fig. 36, shows that τ_{us}^{-1} is at least 20 times larger than τ^{-1}. This discrepancy appears to be larger than can be explained by the fact that τ^{-1} is an average over the phonon modes and directions of propagation.

Similar discrepancies were also noted by Kwok (Kw66) in Ge crystals doped with the donors Sb, As, and P. Kwok explained the very strong ultrasonic attenuation observed by Pomerantz (Po65) at the angular frequency $\omega=2\pi\times9\times10^9$ sec^{-1} through an inelastic process involving both a quantum of ultrasonic energy and a thermal phonon. Conceivably, the same inelastic mechanism is also responsible for the ultrasonic attenuation in KCl:Li. The only drawback of this theory is that it yields a frequency-independent attentuation, in contrast to the experimental findings in KCl:Li. We conclude that although the interaction of ultrasound and of thermal phonons with the tunneling states can be explained qualitatively through the interaction of the oscillating stress with the elastic dipole of the defect, the details of this process, in particular its quantum mechanical aspects, are still not well understood. More work, in particular, scattering experiments, using monochromatic phonons in the frequency range of the tunneling frequencies will be needed.

B. Dielectric Properties. Electric Cooling and Cooperative Phenomena

The use of ac dielectric measurements for the study of the polarization of tunneling states has been mentioned in Chapter V. In this section, we want to discuss cooling by adiabatic depolarization, and also the occurrence of cooperative electric dipole interactions.

If the entropy of a thermodynamic system can be changed by heating or cooling, the system can be used for adiabatic cooling. In addition to the well-known cooling by adiabatic expansion of an ideal gas, or by adiabatic demagnetization of a spin system (Ki66), we want to mention one other example which has been known for a long time and which employs a mechanical force: The entropy of a rubber band is determined by the thermal motion and by the disorder of its long chain molecules. Adiabatic stretching will increase the order of the molecules and hence heat the band. Conversely, adiabatic removal of the stress will lower the temperature of the band. This phenomenon, which is called the Gough–Joule effect after its discoverors, is discussed by Treloar (Tr49).

The feasibility of low-temperature elastic cooling was recently predicted by Känzig (Ka62a) when he discovered the paraelastic behavior of O_2^- ions dissolved in alkali halides. Elastic cooling has since been found in KCl:OH (SF65) at temperatures near 1°K.

Cooling by adiabatic depolarization employing impurity ions with permanent electric dipoles was first studied by Kuhn and Lüty (KL65). In KCl:OH, they observed reversible cooling upon removal of an electric field. The cooling ΔT was proportional to n_{OH}, the square of the initial electric field E_i, and the inverse fourth power of the initial temperature T_i. Kuhn and Lüty explained this with the picture of classical electric dipoles of moment p_0, whose polarization followed a Langevin–Debye law. Equating the electric energy stored in the dipole system, $\int EdP$, to the change of the thermal energy $\int C_v dT=\int AT^3dT$ of the sample, they calculated the cooling ΔT produced by adiabatic depolarization from the initial field E_i for $\Delta T\ll T_i$ and $p_0E_i\ll k_BT_i$:

$$\Delta T=n_{\text{OH}}p_0^2E_i^2/6Ak_BT_i^4, \tag{44}$$

in agreement with the experimental finding. p_0 determined from this experiment agreed with the dipole moment obtained from electric field induced dichroism of the uv band of the OH^- ion (KL64). Shepherd and Feher (SF65, Sh67) extended these measurements to high fields, $p_0E_i\gtrsim kT_i$, and observed the limiting influence of the zero-field tunnel splitting Δ_0 of the OH^- ion on the cooling. A discussion of these results is given by Lawless (La69). Anisotropy of the electric cooling resulting from the fact that the impurity ions have equilibrium positions pointing in the ⟨100⟩ crystallographic orientations has also been observed (Sh67, KL68).

A detailed study of the electric cooling with polarizable impurities, covering starting temperatures T_i and starting fields E_i both larger and smaller than Δ_0/k_B and k_BT/p_0, respectively, and also exploring the anisotropy of the cooling in the limit that $p_0E_i\gg kT_i$, has recently been made on KCl:Li (PTG69, Ta68). The electric cooling was computed starting from the condition of an adiabatic process, $\Delta S=0$:

$$S(E_i, T_i)=S(0, T_f). \tag{45}$$

The entropy $S(E, T)$ was computed using the known electric field dependence of the lithium tunneling states, see Eqs. (18)–(22). Figure 42 shows the good agreement between predicted and observed cooling in KCl:Li. The optimum cooling falls short of the "ideal cooling," defined as $T_f=0$. This is a result of the finite zero-field splitting.

The influence of the zero-field splitting on the electric cooling was also demonstrated on RbCl:CN (PTG69). Here $\Delta_0=0.16$ cm^{-1}, i.e., 5 times smaller than in KCl:Li,

and consequently cooling to much lower temperatures (as low as 0.04°K) was observed.

The electrocaloric effect has been used by Lüty and coworkers (Lu67) to determine the dipole–lattice relaxation time t of tunneling defects. When the electric field is removed in a time comparable to t, the cooling ΔT should decrease, and for times short compared to t, ΔT should approach a very small value, given by the zero-field splitting. Similarly, rapid application of the field should increase the heat generated, and for charging times shorter than t, the heating should be doubled, since now all the phonons will be generated out of the tunneling states split by the maximum electric field. Figure 43 shows some of the data obtained on OH^- doped crystals. From these measurements, relaxation times t between 10^{-5} sec (for RbCl:OH and KBr:OH) and less than 10^{-8} sec (for KI:OH and NaCl:OH) were determined. Some of these times can be found below in Table I. Note that for the shortest discharge times ($t_{\text{disch}} < 10^{-7}$ sec) the RbCl:OH sample actually

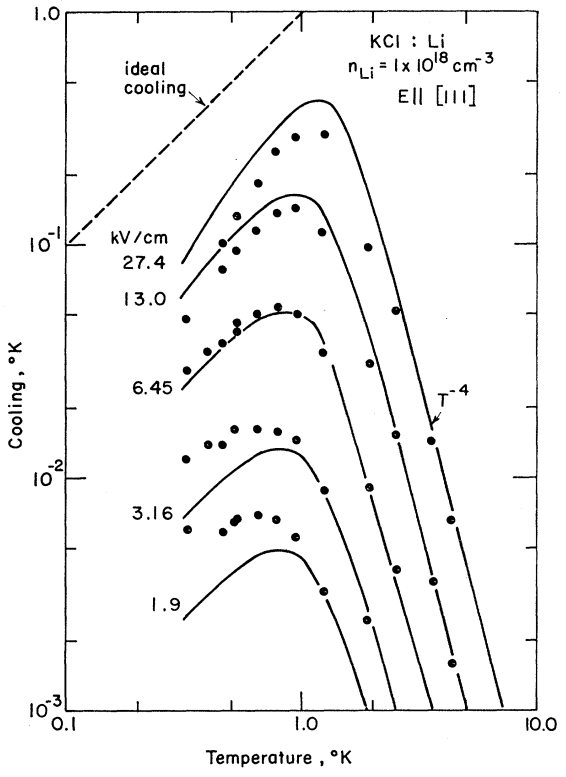

FIG. 42. Electric cooling of KCl:Li (PTG69). E is the applied electric field. $E \parallel [111]$. $n_{Li} = 1 \times 10^{18}$ cm^{-3}. Curves are computed, see text. Note that in the limit of high temperature and low field, the cooling derived from Eq. (45) is isotropic and is given by Eq. (44), in agreement with experiment. The dashed line, called ideal cooling, indicates $\Delta T = -T_i$. At low temperatures and low fields, the observed cooling exceeds the predicted cooling. It is believed that this is caused by lithium ions whose tunneling states are spaced by less than Δ_0 because of random internal stresses, see Fig. 25. At large electric fields and low temperatures, electric field induced ferroelectric ordering of the ions may cause some irreversibility and hence less cooling; see Fi69 and text.

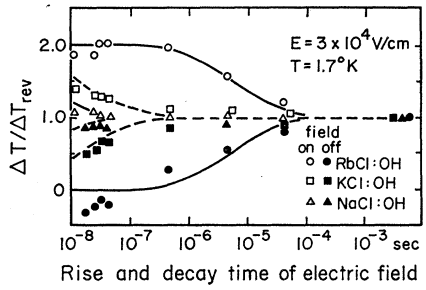

FIG. 43. Dependence of the electric cooling and heating on the time during which the field is removed or applied, after Lu67. $E \parallel [100]$.

heats. The reason for this is not understood. Theoretical efforts (Di68, Vr67) to understand the observed times so far have not given satisfactory agreement with experiment (PHP69a).

The usefulness of the electrocaloric effect for practical low-temperature cooling will depend on whether even smaller zero-field splittings can be found. There are, however, other important limitations: From measurements of the phonon resonance scattering, it was concluded that the dipole–lattice relaxation time decreases with decreasing resonance frequency (Po68), approximately as ω_0^2. Some of these lifetimes can be found in Table I in Chapter VI.D. Hence, as Δ_0 gets smaller, the dipole–lattice relaxation time may get too large. Since the coupling of the tunneling states to the lattice is very strong, this appears to be a minor problem, in contrast to spin systems. Another limitation seems to be the random internal stresses, which are expected to produce a lower limit to the splitting of the low-energy motional states, as discussed in V.F.

Another limitation of the cooling should be electric or elastic dipole–dipole interaction, which should ultimately produce an ordered state. The influence of electric dipole interaction on the cooling has been suspected in KCl:OH near 1°K (Sh67, La69), and also in KCl:Li (PTG69).

No such influence has been observed in RbCl:CN at temperatures as low as 0.04°K (PTG69). Since the electric dipole moment of CN^- is 10 times smaller than that of OH^- and Li^+ and since any dipole–dipole interaction goes as the square of the dipole moment, the CN^- ion appears to be a more promising candidate for practical low-temperature cooling (PTG69). This point has recently been discussed by Lawless (La69a), who compared magnetic, electric, and dilution refrigeration.

The first observation of electric dipole interaction was made by Känzig, Hart, and Roberts in an investigation of the low-temperature ac (10^2–10^4 Hz) dielectric constant of KCl:OH (KHR64). Instead of approaching a saturation value characteristic of the polarizability of the lowest tunneling state, the real part of the defect induced dielectric constant went through a maximum at a temperature T_{max}, which

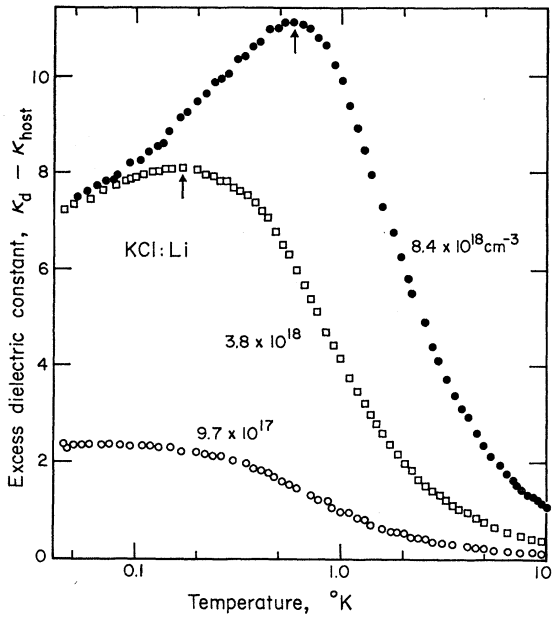

FIG. 44. Defect induced dielectric constant $\Delta\kappa=\kappa_d-\kappa_{\rm host}$ of KCl:Li, after Fiory (Fi69). At the lowest concentration, $\Delta\kappa$ agrees with the theory based on the polarization of the individual Li^+ tunneling states, with a tunnel splitting $\Delta_0=0.73$ cm^{-1}, only 10% smaller than the correct value and in good agreement with the measurements of the ac dielectric constant by Bogardus and Sack (S66b). At the higher concentrations, agreement with this theory is found only at high temperatures ($T>5$°K). The arrows indicate the temperatures $T_{\rm max}$.

scaled with the OH^- concentration. This was taken as evidence for an electric dipole interaction. $T_{\rm max}$, however, also shifted to lower temperatures for lower measuring frequencies, indicating a slow relaxation process. It has recently been demonstrated by Fiory (Fi69) that a similar maximum of the dielectric constant also occurs in dc measurements, but at a somewhat lower temperature. Fiory also extended these measurements to other dipolar impurities, namely to Li^+ in KCl, OH^- in RbCl, and F^- in NaBr. Figure 44 shows the results he obtained on KCl:Li. He found that the temperature of the maximum for all defects is proportional to the product of the square of the dipole moment p_0 times the defect concentration n, as shown in Fig. 45. A good fit to the data could be obtained with the following expression:

$$T_{\rm max}=np_0^2/(4\pi\kappa_{\rm host}\epsilon_0 k_B), \qquad (46)$$

where p_0 is uncorrected for the local electric field, $\kappa_{\rm host}$ is the dielectric constant of the host crystal, and $\epsilon_0=8.86\times10^{-12}$ amp·sec/V·m is the permittivity of free space. This observation indicated strongly that the low-temperature behavior is indeed caused by an electric dipole interaction.

Känzig, Hart, and Roberts (KHR64) suggested that the maximum in the dielectric constant resulted from a transition to a ferroelectrically ordered state. They estimated the transition temperature from the Clausius–Mossotti expression relating atomic polarizability α and dielectric constant κ:

$$(\kappa-1)/(\kappa+2)=(1/3\epsilon_0)\sum_i n_i\alpha_i, \qquad (47)$$

where n is the number density of the ith species of atoms (or molecules). If κ_d is the dielectric constant of the doped crystal, $\kappa_{\rm host}$ that of the pure crystal, Eq. (47) can be written as

$$\frac{n\alpha}{3\epsilon_0}=\frac{\kappa_d-1}{\kappa_d+2}-\frac{\kappa_{\rm host}-1}{\kappa_{\rm host}+2}, \qquad (48)$$

where n and α refer to the impurities. For the polarizability they assumed a Langevin–Debye law:

$$\alpha=\frac{[3p_0/(\kappa_{\rm host}+2)]^2}{3k_BT}.$$

The expression in brackets is the dipole moment corrected assuming a Lorentz local field. The onset of ferroelectricity is characterized by $\kappa_d\to\infty$. Thus Eq. (48) defines a critical temperature $T_{\rm KHR}$ (KHR64)

$$T_{\rm KHR}=np_0^2/\{(\kappa_{\rm host}+2)3\epsilon_0 k_B\}.$$

$T_{\rm KHR}$ defined by the above equation agrees quite well with the experimental $T_{\rm max}$, see Fig. 45. An exten-

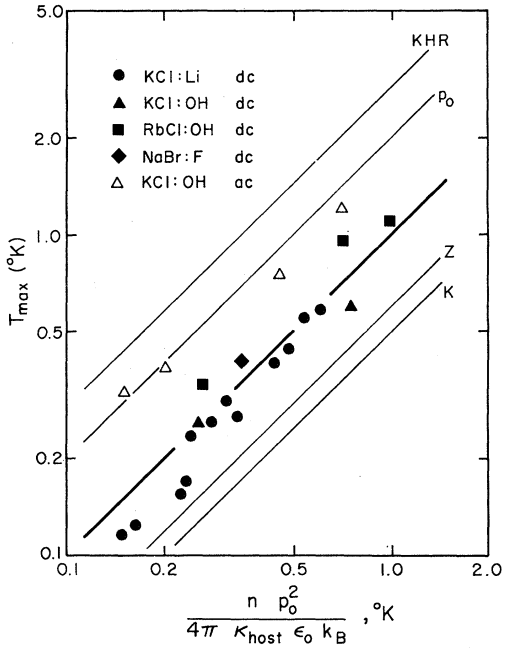

FIG. 45. Temperature $T_{\rm max}$, at which the maximum dielectric constant is observed, plotted against np_0^2. Solid symbols: dc measurements on KCl:Li, KCl:OH, RbCL:OH, and NaBr:F, after Fiory. Open triangles: ac measurements (10^3 Hz) by Känzig *et al.* (KHR64). The dc data fall very close to the heavy solid line, representing (the empirical) Eq. (46). The line labeled KHR is the critical temperature, Eq. (48), after KHR64; the line labeled K is based on Klein's theory, Eq. (4.9, bottom) of K166. The line labeled Z was obtained by Zernik (Ze65), and the one labeled p_0 is the critical temperature given by the interaction of two dipoles, Eq. (49). The critical temperatures according to Lawless (La66) and to Baur and Salzman (BS69) fall close to the line labeled p_0.

sion of these ideas along the theory of Onsager (On36) and Pirenne (Pi49) for dipolar systems in which spontaneous ferroelectric ordering can occur was given by Zernik (Ze65). His critical temperatures T_Z are also close to the experimental data.

Brout (Br65) and Klein (Kl66) studied the interaction between randomly distributed electric dipoles using a technique developed earlier for dilute magnetic systems (KB63, Kl63) and found that the majority of the dipoles will align antiparallel. They concluded that the maximum in the dielectric constant marks the onset of antiferroelectric ordering; their critical temperatures also were found to be close to the experimental ones. Klein's critical temperature T_K is also shown in Fig. 45. Similar results were obtained by Lawless (La66), who made a machine calculation of the interaction energy of the randomly distributed dipoles. His critical temperatures were just 20% smaller than the T_{KHR} determined from the model of Känzig *et al.* All of these calculations were done using classical electric dipoles. Baur and Salzman (BS69) formally included the quantum mechanical nature of the tunneling states. For KCl:OH, their results agree well with the classical calculations. In KCl:Li, however, they did not obtain a maximum in the dielectric constant up to concentrations exceeding 2×10^{19} cm^{-3}, in contrast to the experiment, see Fig. 44.

Fiory has also studied the ferroelectric polarization of electric dipole systems at high fields in the region below $T_{\max}$. He found that at sufficiently high electric fields all the dipoles observed in the paraelectric region can be aligned even at the lowest temperatures, and also observed a remnant polarization decaying logarithmically with time. His experiments can be understood with Brout's model that the ground state of the dilute dipolar system is indeed one of local antiferroelectric order within clusters of two to three dipoles (Fi69).

The observed critical temperatures $T_{\max}$ can also be explained by considering the interaction energy of just two dipoles. According to Frohlich (Fr58), the energy of interaction between two dipoles p_0 separated by the distance r in a host of dielectric constant κ_{host} is

$$W_{p_0}=p_0^2/(2\pi\kappa_{\mathrm{host}}\epsilon_0 r^3). \tag{49}$$

p_0 is the uncorrected dipole moment, as obtained from experiment (Fr58, Appendix A2). Assuming r to be the average distance between the dipoles in the crystal, $r^3 = n^{-1}$, a critical temperature T_{p_0} is defined by

$$W=k_B T_{p_0}. \tag{50}$$

Then,

$$T_{p_0}=np_0^2/(2\pi k_{\mathrm{host}}\epsilon_0 k_B). \tag{51}$$

It is seen in Fig. 45 that T_{p_0} also gives a good description of the experiment, differing from Eq. (46) only by a factor of 2. It is remarkable that even such a simple model yields a critical temperature close to the observed one. The critical concentrations n_{c,p_0}, defined as the concentration at which $T_{p_0}=1$°K, can be found in Table I (Chapter VI.D) for KCl:OH$^-$, KCl:Li$^+$, and KCl:CN$^-$. These values allow one to estimate the concentrations for which cooperative effects should become noticeable at a given temperature.

For a comparison, Table I also lists the critical concentrations, n_{c,p_λ}, at which the elastic dipole–dipole interaction energy equals 1°K k_B, computed using elastic dipole theory (NH65). Except for CN$^-$, the elastic interaction appears to be weaker than the electric one. Elastic dipole ordering has not been observed so far. We refer to the study of the elastic properties of Li$^+$ and CN$^-$ by Byer and Sack (HPP68a, BS68) and to the specific-heat work by Peressini *et al.* (PHP69a).

Evidence for an electric interaction between tunneling defects has also been found in other experiments, as, for instance, in specific heat (PHP69a), thermal conductivity (PHP69, Ro68, RCK69), far-infrared absorption (KS69), and also in measurements of the electro-optical, elasto-optical, and electrocaloric effects in OH$^-$ doped crystals at high concentrations (LU67). Although in none of these experiments was the transition to an ordered state as clear as in the dielectric measurements, it appears that a theoretical study of these observations should contribute significantly to our understanding of the dipolar interaction. The only theoretical work presently available is that by Lawless (La66), who studied the specific heat connected with the ordering of classical dipoles and found it to be proportional to T^{-1}. The excess specific heat observed (PHP69a) in KCl containing large concentrations of OH$^-$ or Li$^+$, however, increases rapidly with increasing temperature; see, for instance, Fig. 31, curve E. The reason for this disagreement is probably that in the calculation the finite tunnel splitting of the motional ground states of the defects had not been included.

C. Phonon Generation. The Conversion of Electromagnetic to Elastic Energy

We have seen that the heat capacity associated with the tunneling states of impurity ions in a crystal is greater by orders of magnitude than that of the lattice vibrations to which the ions are coupled. We have also seen that because of their large electric and elastic dipole moments these ions couple very strongly with microwaves and phonons possessing the right energy. At low temperatures, when the mean free path of the phonons in the absence of the paraelectric ions is large, it should be possible to efficiently generate ballistic pulses of monochromatic phonons by excitation of the tunneling states with resonant microwaves.

The problem discussed here is in many ways analogous to the well-known problem of the phonon bottleneck for spin systems. Several investigators have cited evidence for the existence of this effect for spin systems (FS61, SJ62, BW65, Sh66, AS68). Recently Brya *et al.* (BGD68) have observed the hot phonons directly by means of Brillouin light scattering. In contrast to spin

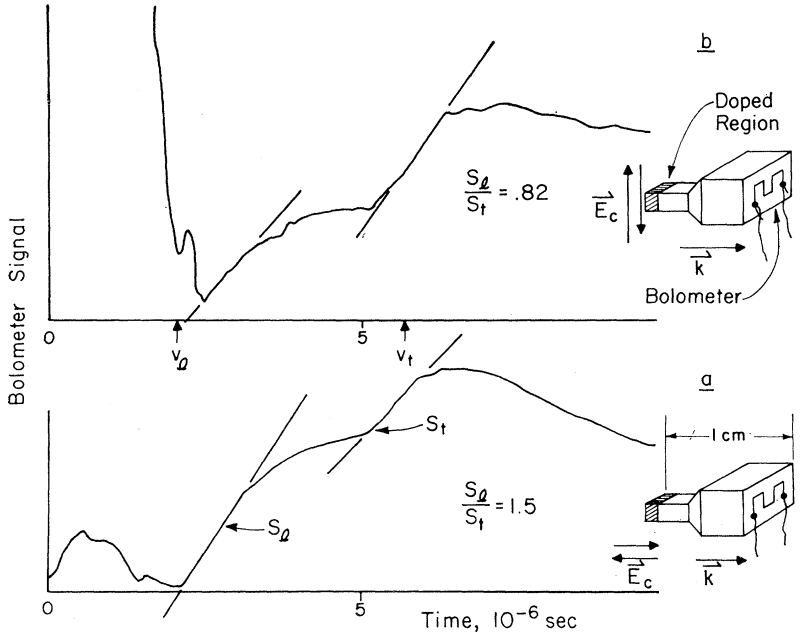

FIG. 46. KCl:Li. Phonon generation using 24 GHz microwaves. $T=1.3$°K. Bolometer signal (obtained using boxcar integrator) with phonon propagation vector $\mathbf{k} \parallel [100]$, parallel to cavity electric field $\mathbf{E}_c$ (case a), and perpendicular to $\mathbf{E}_c$ (case b). S_ℓ and S_t are longitudinal and transverse slopes and are a qualitative measure of the elastic power. Distortion of field by cavity port prevented complete discrimination between $\mathbf{E}_c \parallel \mathbf{k}$ and $\mathbf{E}_c \perp \mathbf{k}$. After CNP69.

systems, paraelectric ions have the advantage of orders of magnitude stronger coupling, to both the microwave photons and phonons. Furthermore, they can be tuned over a wide range of frequencies with modest electric fields.

Phonon generation employing tunneling states has been demonstrated by Channin *et al.* (CNP69), who pumped one end of a KCl crystal containing Li^+ ions diffused into a thin layer at one end, Fig. 46, with microsecond pulses of 24-GHz-microwave photons and detected the phonons arriving at the other end with a superconducting bolometer. From the time-of-flight measurements the modal dependence of the generated phonons could be studied. With the cavity electric field $\mathbf{E}_c$ parallel to the phonon propagation direction, Fig. 46(a), the relative intensity of the longitudinal to transverse phonons is 1.5 while, with the field perpendicular, Fig. 46(b), the ratio is 0.8. This angular dependence of the relative intensity and the ballistic arrival times of the phonons provides strong evidence that the phonons did not come from a thermal process and had not suffered multiple scattering in transit. Preliminary measurements of the influence of Stark splitting of the tunneling states showed that the generated phonons were created by a resonant excitation of these states by the microwaves.

In Chapter VI.A we saw that the thermal conductivity measurements of Walton (Wa67) and of Peressini *et al.* (PHP69) showed that the phonons couple strongly with both the even–even and the even–odd transitions. Since only the A_{1g} and T_{1u} states are thermally populated and the 24 GHz microwaves couple only neighboring tunneling states, at 1.3°K, the temperature of Channin's experiment, the generated phonons should have the energy Δ_0 or $2\Delta_0$. The triplet T_{1u} consists of the three states T_{1ux}, T_{1uy}, and T_{1uz}, where the z direction is defined by the microwave electric field $\mathbf{E}_c$. Since $\mathbf{E}_c$ couples only to T_{1uz}, one expects that as far as the generation of phonons of energy Δ_0 is concerned, longitudinal waves are preferentially generated for $\mathbf{E}_c \parallel \mathbf{k}$, while transverse waves are emitted for $\mathbf{E}_c \perp \mathbf{k}$, as is indeed found in the experiment.

The measurements of Channin *et al.* show for the first time the feasibility of studying the phonon-defect interaction of paraelectric ions by means of microwave excitation as a function of phonon polarization, direction of propagation, and electric fields. It would also be of great interest to determine the precise bandwidth of the generated phonons. It appears feasible to study this by using a spin system as a monitor (AS68) or by means of Brillouin light scattering (BGD68).

D. Summary of Data Regarding Tunneling States

For a compilation of the tunnel splittings determined for KCl:CN, KBr:CN, KI:CN, RbCl:CN, KCl:OH, KCl:^{7}Li, and KCl:^{6}Li we refer to Fig. 37. In Table I we list some data concerning the elastic and electric properties of the tunneling states.

ω_0 is the phonon angular frequency at which resonance scattering was observed in thermal conductivity. A is the scattering strength as defined through Eq. (34), determined from best fits to the thermal conductivity (Po68). For KCl:OH, see the caption of Fig. 41, as well as CKW67, Ro68, RCK69.

p_λ is the elastic dipole moment, defined through Eq. (28). Data for OH^- doped KCl, KBr, and RbCl is from HL65, Ha66; for KCl:Li, HPP68a; for CN^-,

TABLE I. Some useful data concerning tunneling states. They are explained in the text of Chapter VI.D.

	ω_0 10^{11} rad/sec	A [Eq. (34)] 10^{12} cm³/sec³	p_λ [Eq. (28)] 10^{-24} cm³	p_0 (debyes)	n_{c,p_λ} 10^{19}/cm³	n_{c,p_0} 10^{19}/cm³	Lifetime (sec) from El. cal.	Diel.	PER	$K(T)$
KCl:OH	~1.1	~0.3	5.9	3.8	11	1.9	10^{-8}	~10^{-8}		7×10^{-9}
RbCl:CN	1.28	1.88		0.3						1.6×10^{-9}
KCl:^{7}Li	2.25	2.37	3.8	6.0	27	0.86	10^{-8}		10^{-9}	1.2×10^{-9}
KCl:^{6}Li	3.27	2.92		6.0						8×10^{-10}
KCl:CN	3.0	10.4	9.4	0.5	4.4	120				4×10^{-10}
KBr:CN	3.0	16.1	17	0.5						2.5×10^{-10}
KI:CN	3.0	5.5	14	0.5						3×10^{-10}
KBr:OH			7.8	~3.8			2×10^{-5}	~10^{-5}		
RbCl:OH			5.0	~3.8			~10^{-5}			

BS68; note, however, that these authors found an elastic dipole tensor with three different principal axes, i.e., three different shape factors; the values listed here are averages. The molecules respond to T_{2g} stress with a large elastic moment, to E_g stress with a small one; the latter was found to agree with the one obtained from E_g stress induced infrared dichroism (SN66).

p_0 is the electric dipole moment, uncorrected for local field. For KCl:OH, KL64; in the other hosts, OH^- has a similar dipole moment (LU67). For the CN^- dipole moment in RbCl, see PTG69; in the potassium hosts, SM65 and H. S. Sack, private communication. For the Li^+ dipole moment, see HPP68a, He68, HS69, KS69.

The critical concentration, n_{c,p_λ} for elastic dipole–dipole interaction, was given for KCl:Li in HPP68a and was estimated for OH^- and CN^- in PHP69.

The critical concentrations for electric dipole–dipole interaction, n_{c,p_0}, defined in Eqs. (49)–(51) in this paper, were obtained in PHP69.

The lifetimes of the tunneling states were determined by four different methods: (a) from the electrocaloric effect, see Fig. 43 (KL68, LU67), at ~1°K and 30 kV cm^{-1}; (b) from dielectric relaxation, by Känzig and co-workers (BDK65, KKP67). The values listed were obtained at 1°K. The reorientation time varied inversely proportional with T up to 10°K; (c) paraelectric resonance (HS69); (d) from thermal conductivity (Po68). This is an indirect method, based on a specific model. Note that the width of the tunneling states appears to be determined by random internal stress and electric fields, and hence cannot be used to determine the lifetime. See the discussion in V.C.

VII. UNSOLVED PROBLEMS AND OUTLOOK

We have seen that the tunneling states associated with atoms and molecules isolated as impurities in crystals have now been well studied by techniques analogous to those performed on spin systems. The static response of such ions to uniaxial stress and electric fields is well understood. The effects, at low temperatures, of the finite zero-field (tunnel) splitting on the dielectric properties of a dilute gas of electric dipoles has been verified for the first time. The effects of electric dipole–dipole interactions (dilute ferroelectricity) have been observed but much work along these lines needs to be done, since for the first time there exists the possibility of studying ferroelectricity as a function of ion concentration in analogy with the work done on dilute magnetic alloys. The dynamics of relaxation and the coupling of paraelectric ions to lattice vibrations is not well understood. More experimental work, using high-frequency monochromatic phonons, and theoretical work to elucidate the nature of the phonon-defect interaction need to be done.

Until the present time almost all of the work on paraelectric ions has been confined to alkali halide matrices. More work needs to be done to find tunneling entities in other materials. Particularly, the discovery of new off-center ions should help in our understanding of the theoretical reasons for the existence of central instabilities in solids. It could prove especially fruitful to relate the problem of central instabilities to the already large body of work done on the Jahn–Teller effect where the distortion of the surrounding ligands, and not the displacement of the central ion, has been the primary consideration.

Finally, the application of tunneling states for practical low-temperature cooling and their use as tunable sources of high-frequency monochromatic phonons need to be explored more fully.

REFERENCES

AC69 Alderman, D. W., and R. M. Cotts (private communication).

Al69 ——, Ph.D. thesis, Cornell University, Materials Science Center Report No. 1052, 1969 (unpublished).

An50 Andrew, E. R., J. Chem. Phys. **18**, 607 (1950).

AS68 Anderson, C. H., and E. S. Sabisky, Phys. Rev. Letters **21**, 987 (1968).

Au68 Auyang, R. P., Ph.D. thesis, Cornell University, Cornell Materials Science Center Report No. 841 1968 (unpublished).

Ba29 Barker, E. F., Phys. Rev. **33,** 684 (1929).

Ba64 Baumann, F. C., Bull. Am. Phys. Soc. **9,** 644 (1964).

BAW62 Bhatnagar, S. S., E. J. Allin, and H. L. Welsh, Can. J. Phys. **40,** 9 (1962).

BBSP63 Brajovic, V., H. Boutin, G. J. Safford, and H. Palevsky, J. Phys. Chem. Solids **24,** 617 (1963).

BD66 Bron, W. E., and R. W. Dreyfus, Phys. Rev. Letters **16,** 165 (1966).

BD67 ——, and R. W. Dreyfus, Phys. Rev. **163,** 304 (1967).

BDK65 Bosshard, U., R. W. Dreyfus, and W. Känzig, Physik Kondensierten Materie **4,** 254 (1965).

Be29 Bethe, H. A., Ann. Physik **3,** 133 (1929).

BF66 Bowers, M. T., and W. H. Flygare, J. Chem. Phys. **44,** 1389 (1966), and references cited therein.

BFK67 Brugger, K., T. C. Fritz, and D. A. Kleinman, J. Acoust. Soc. Am. **41,** 1015 (1967).

BGD68 Brya, W. J., S. Geschwind, and G. E. Devlin, Phys. Rev. Letters **21,** 1800 (1968).

BGKM66 Bowen, S. P., M. Gomez, J. A. Krumhansl, and J. A. D. Matthew, Phys. Rev. Letters **16,** 1105 (1966).

BHPS67 Baumann, F. C., J. P. Harrison, R. O. Pohl, and W. D. Seward, Phys. Rev. **159,** 691 (1967).

BKW69 Breen, D. P., D. C. Krupka, and F. I. B. Williams, Phys. Rev. **179,** 241 (1969).

BM61 Brugger, K., and W. P. Mason, Phys. Rev. Letters **7,** 270 (1961).

BMR65 Burgiel, J. C., H. Meyer, and P. L. Richards, J. Chem. Phys. **43,** 4291 (1965). This paper deals with the far-ir absorption in several clathrates.

BP68 Bird, B. L., and N. Pearlman, in *Proceedings of the Seventh Conference on Thermal Conductivity*, D. R. Flynn and B. A. Peavy, Jr., Eds. (National Bureau of Standards, Washington, D.C., 1968), Spec. Publ. No. 302, p. 103.

Br65 Brout, R., Phys. Rev. Letters **14,** 175 (1965).

BS66 Baur, M. E., and W. R. Salzman, Phys. Rev. **151,** 710 (1966).

BS66a Bogardus, H., and H. S. Sack, Bull. Am. Phys. Soc. **11,** 229 (1966).

BS66b ——, and H. S. Sack, Footnote 3 in LS66.

BS68 Byer, N. E., and H. S. Sack, Phys. Status Solidi **30,** 569, 579 (1968).

BS68a ——, and H. S. Sack, J. Phys. Chem. Solids **29,** 677 (1968).

BS69 Baur, M. E., and W. R. Salzman, Phys. Rev. **178,** 1440 (1969).

Bu13 Burmeister, W., Verhandl. Deut. Physik. Ges. **15,** 589 (1913).

BW65 Brya, W. J., and P. E. Wagner, Phys. Rev. Letters **14,** 431 (1965); Phys. Rev. **157,** 400 (1967).

Ca59 Callaway, J., Phys. Rev. **113,** 1046 (1959).

Ca62 Carruthers, P., Bull. Am. Phys. Soc. **7,** 16 (1962).

CBG63 Coogan, C. K., G. G. Belford, and H. S. Gutowsky, J. Chem. Phys. **39,** 3061 (1963).

CG64 ——, and H. S. Gutowsky, J. Chem. Phys. **40,** 3419 (1964).

Ch69 Chase, L. L., Phys. Rev. Letters **23,** 275 (1969).

CKW67 Chau, C. K., M. V. Klein, and B. Wedding, Phys. Rev. Letters **17,** 371 (1967).

CNP69 Channin, D. J., V. Narayanamurti, and R. O. Pohl, Phys. Rev. Letters **22,** 524 (1969).

CNS67 Clayman, B. P., I. G. Nolt, and A. J. Sievers, Phys. Rev. Letters **19,** 111 (1967).

Co51 *Tables Relating to the Mathieu Functions* (Columbia University Press, New York, 1951), p. 44.

CSH63 Cabana, A., G. B. Savitsky, and D. F. Hornig, J. Chem. Phys. **39,** 2942 (1963).

Cu38 Cundy, H. M., Proc. Roy. Soc. (London) **A164,** 420 (1938).

CW34 Cleeton, C. E., and N. H. Williams, Phys. Rev. **45,** 234 (1934).

De29 Debye, P., *Polar Molecules* (The Chemical Catalog Company, MM, 1929; reprinted by Dover Publications, New York, 1929), p. 102ff.

De36 Devonshire, A. F., Proc. Roy. Soc. (London) **A153,** 601 (1936).

DF66 Dreybrodt, W., and K. Fussgänger, Phys. Status Solidi **18,** 133 (1966).

DHSW66 Dienes, G. J., R. D. Hatcher, R. Smoluchowski, and W. Wilson, Phys. Rev. Letters **16,** 25 (1966).

Di68 Dick, B. G., Phys. Status Solidi **29,** 587 (1968).

DM65 For recent work see S. A. Dickson and H. Meyer, Phys. Rev. **138,** A1293 (1965).

Dr68 Dreyfus, R. W., J. Phys. Chem. Solids **29,** 1941 (1968).

Dr69 ——, Solid State Commun. **7,** 827 (1969).

EP58 Etzel, H. W., and D. A. Patterson, Phys. Rev. **112,** 1112 (1958).

Er24 Errera, J., J. Phys. Radium **5,** 304 (1924).

Es68 Estle, T. L., Phys. Rev. **176,** 1056 (1968).

Eu39 Eucken, A., Z. Electrochem. **45,** 126 (1939).

Ew62 Ewing, G., J. Chem. Phys. **37,** 2250 (1962).

Ew64 ——, J. Chem. Phys. **40,** 179 (1964).

FAL63 Fritz, B., J. Anger, and F. Lüty, Z. Physik **174,** 240 (1963).

Fe65 Feynman, R. P., *Lectures on Physics* (Addison–Wesley, Reading, Mass., 1965), Vol. 3, Chaps. 7 and 8.

FG65 Fischer, F., and H. Gründig, Z. Physik **184,** 299 (1965).

Fi64 ——, Solid State Commun. **2,** 51 (1964).

Fi69 Fiory, A. T., Bull. Am. Phys. Soc. **14,** 346 (1969), and Cornell Material Science Center, Report No. 1277, 1970.

FJ67 Facey, O. E., and P. W. M. Jacobs, Phys. Status Solidi **19,** 565 (1967).

Fo35 Fowler, R. H., Proc. Roy. Soc. (London) **A149,** 1 (1935).

Fr46 Frenkel, J., *Kinetic Theory of Liquids* (Oxford University Press, London, 1946), Chap. II. See particularly pp. 80–92 and references cited therein.

Fr58 Fröhlich, *Theory of Dielectrics* (Oxford University Press, Oxford, England, 1958), 2nd ed.

Fr62 Fritzsche, H., Phys. Rev. **125,** 1560 (1962).

FS61 Faughnan, B. W., and M. W. P. Strandberg, J. Phys. Chem. Solids **19,** 155 (1961).

FSS66 Feher, G., I. W. Shepherd, and H. B. Shore, Phys. Rev. Letters **16,** 500 (1966).

Ga28 Gamow, G., Z. Physik **51,** 204 (1928).

GBK67 Gomez, M., S. P. Bowen, and J. A. Krumhansl, Phys. Rev. **153,** 1009 (1967).

GC28 Gurney, R. W., and E. U. Condon, Nature **122,** 439 (1928); also Phys. Rev. **33,** 127 (1929).

GC63 Griffin, A., and P. Carruthers, Phys. Rev. **131,** 1971 (1963).

GHAW60 Gush, H. P., W. F. J. Hare, E. J. Allin, and H. L. Welsh, Can. J. Phys. **38,** 176 (1960).

GJ28 Giauque, W. F., and K. Johnston, J. Am. Chem. Soc. **50,** 322 (1928).

GP50 Gutowsky, H. S., and G. E. Pake, J. Chem. Phys. **18,** 162 (1950).

GP50a Reference GP50, p. 257.

GP61 J. F. Goff and N. Pearlman, in *Proceedings of the 7th International Conference on Low Temperature Physics*, edited by G. N. Graham and A. C. Hollis Hullet (University of Toronto Press, Toronto, 1961), pp. 284–288 and Phys. Rev. **140,** A2151 (1965).

GPB54 Gutowsky, H. S., G. E. Pake, and R. Bersohn, J. Chem. Phys. **22,** 643 (1954).

GPB54a ——, G. E. Pake, and R. Bersohn, J. Chem. Phys. (1954).

HA60 Hrostowski, H. J., and F. J. Alder, J. Chem. Phys. **33,** 480 (1960).

Ha60 Hasegawa, H., Phys. Rev. **118,** 1523 (1960).

Ha66 Härtel, H., Ph.D. thesis, Stuttgart University, Germany, 1966

Ha68 Harrison, J. P., Rev. Sci. Instr. **39,** 145 (1968).

HBW67 Höcherl, G., D. Blumenstock, and H. C. Wolf, Phys. Letters **24A,** 511 (1967).

HD56 Hexter, R. M., and D. M. Dows, J. Chem. Phys. **25,** 204 (1956).

He58 ——, Spectrochim. Acta **10,** 291 (1958).

He68 Herendeen, R. A., Bull. Am. Phys. Soc. **13,** 660 (1968).

HL65 Härtel, H., and F. Lüty, Phys. Status Solidi **12,** 347 (1965).

HL68 ——, and F. Lüty, International Color Center Conference, Rome, 1968 (unpublished).

HLP68 Harrison, J. P., G. Lombardo, and P. P. Peressini, J. Phys. Chem. Solids **29,** 557 (1968).

HPP68 ——, P. P. Peressini, and R. O. Pohl, Phys. Rev. **167,** 856 (1968).

HPP68a ——, P. P. Peressini, and R. O. Pohl, Phys. Rev. **171,** 1037 (1968).

HPP68b ——, P. P. Peressini, and R. O. Pohl, in *International Conference on Localized Excitations*, R. F. Wallis, Ed., (Plenum Press, Inc., New York, 1968), p. 474.

HR49 Hatton, J., and B. V. Rollin, Proc. Roy. Soc. (London) **A199,** 222 (1949).

HR54 Hill, R. W., and B. W. A. Ricketson, Phil. Mag. **45,** 277 (1954).

HS69 Herendeen, R. A., and R. H. Silsbee, Phys. Rev. **188,** 645 (1969).

HSMcT69 Hardy, W. N., I. F. Silvera, and J. P. McTague, Phys. Rev. Letters **22,** 297 (1969).

Hu27 Hund, F., Z. Physik, **43,** 805 (1927).

Hu69 Huiskamp, W. J., (private communication).

HW68 Höcherl, G., and H. C. Wolf, Phys. Letters **27A,** 133 (1968).

HW69 Hetzler, M., and D. Walton (private communication).

Je60 Jen, C. K., in *Formation and Trapping of Free Radicals*, A. M. Bass and H. P. Broida, Eds. (Academic Press, 1960.

Ka62 Känzig, W., J. Phys. Chem. Solids **23,** 479 (1962).

Ka62a Reference Ka62, p. 496.

KB63 Klein, M. W., and R. Brout, Phys. Rev. **132,** 2412 (1963).

Ke61 Keyes, R. W., Phys. Rev. **122,** 1171 (1961).

KH66 King, H. F., and D. F. Hornig, J. Chem. Phys. **44,** 4520 (1966).

KHR64 Känzig, W., H. R. Hart, and S. Roberts, Phys. Rev. Letters **13,** 543 (1964).

KHS68 Kirby, R. D., A. E. Hughes, and A. J. Sievers, Phys. Letters **28A,** 170 (1968).

Ki60 King, H. F., Ph.D. thesis, Princeton University, 1960 (unpublished).

Ki62 Kittel, C., *Introduction to Solid State Physics* (John Wiley & Sons, Inc., New York, 1962), 2nd ed., Chap. 6.

Ki66 ——, *Introduction to Solid State Physics* (John Wiley & Sons, New York, 1966), 3rd ed., Chap. 14.

KKGW68 Klein, M. V., S. O. Kennedy, T. I. Gie, and B. Wedding, Mat. Res. Bull. **3,** 677 (1968).

KKP67 Känzig, W., K. Knop, and G. Pfister, Helv. Phys. Acta **40,** 825 (1967).

Kl61 Klein, M. V., Phys. Rev. **122,** 1393 (1961).

Kl61a ——, Ph.D. thesis, Cornell University, Cornell Materials Science Center Report No. 1, 1961, p. 143.

Kl63 ——, Phys. Rev. Letters **11,** 408 (1963).

Kl66 ——, Phys. Rev. **141,** 489 (1966).

KL68 Kapphan, S., and F. Lüty, Solid State Commun. **6,** 907 (1968).

KL64 Kuhn, U., and F. Lüty, Solid State Commun. **2,** 281 (1964).

KL65 ——, and F. Lüty, Solid State Commun. **4,** 31 (1965).

KNAS68 Kirby, R. D., I. G. Nolt, R. W. Alexander, and A. J. Sievers, Phys. Rev. **168,** 1057 (1968).

Ko57 Kohn, W., in *Solid State Physics*, F. Seitz and D. Turnbull, Eds. (Academic Press Inc., New York, 1957), Vol. 5.

Ko65 Köstlin, H., Solid State Commun. **4,** 81 (1965).

KPH31 Karacek, F. C., E. Posjnak, and S. B. Hendriks, J. Am. Chem. Soc. **53,** 1185 (1931).

Kr65 Krumhansl, J. A., Proc. Phys. Soc. (London) **85,** 921 (1965).

KS69 Kirby, R. D., and A. J. Sievers, Bull. Am. Phys. Soc. **14,** 301 (1969); R. D. Kirby, Ph.D. thesis, Cornell University, Cornell Materials Science Center Report No. 1122, 1969 (unpublished).

KSV69 Kumar, A., A. K. Srivastava, and G. S. Verma, Phys. Rev. **178,** 1480, 1488 (1969).

Kw66 Kwok, P. C., Phys. Rev. **149,** 666 (1966).

KWL69 Klein, M. V., B. Wedding, and M. A. Levine, Phys. Rev. **180,** 902 (1969).

La37 Landau, L., Physik-Z. Sowjetunion **11,** 26, 545 (1937).

La49 Lander, J. J., J. Chem. Phys. **17,** 892 (1949).

La66 Lawless, W. N., Physik Kondensierten Materie **5,** 100 (1966).

La69 ——, J. Phys. Chem. Solids **30,** 1161 (1969).

La69a ——, J. Appl. Physics **40,** 4448 (1969).

Lo70 Lombardo, G., Ph.D. thesis, Cornell University, 1970 (unpublished).

LP53 Levy, H. A., and S. W. Peterson, J. Am. Chem. Soc. **75,** 1536 (1953).

LP65 ——, and R. O. Pohl, Phys. Rev. Letters **15,** 291 (1965).

LP66 ——, and R. O. Pohl, Bull. Am. Phys. Soc. **11,** 212 (1966).

LS66 Lakatos, A., and H. S. Sack, Solid State Commun. **4,** 315 (1966).

Lu67 Lüty, F., J. Phys. (Colloque C4) **28,** C4-120 (1967).

Ma65 Matthew, J. A. D., Solid State Comm. **3,** 365 (1965).

Me61 Merzbacher, E., *Quantum Mechanics* (John Wiley & Sons, New York, 1961), Chap. 5.

Me61a Meyer, H., J. Phys. Chem. Solids **20,** 238 (1961).

MHD61 Milligan, D. E., R. M. Hexter and K. Dressler, J. Chem. Phys. **34,** 1009 (1961).

MOV57 Meyer, H., N. C. M. O'Brien, and J. H. Van Vleck, Proc. Roy. Soc. (London) **A243,** 414 (1957).

MS59 ——, and T. A. Scott, J. Phys. Chem. Solids **11,** 215 (1959).

MZ41 Messer, C. E., and W. T. Ziegler, J. Am. Chem. Soc. **63,** 2703 (1941).

Na64 Narayanamurti, V., Phys. Rev. Letters **13,** 693 (1964).

NH63 Nowick, A. S., and W. R. Heller, Advan. Phys. **12,** 251 (1963).

NH65 ——, and W. R. Heller, Adv. Phys. **14,** 101 (1965).

Ni35 Nielsen, H. H., J. Chem. Phys. **3,** 189 (1935).

No27 Nordheim, L., Z. Physik **46,** 833 (1927).

NS66 Nolt, I. G., and A. J. Sievers, Phys. Rev. Letters **16,** 1103 (1966).

NS68 ——, and A. J. Sievers, Phys. Rev. **174,** 1004 (1968).

NSP66 Narayanamurti, V., W. D. Seward, and R. O. Pohl, Phys. Rev. **148,** 481 (1966).

On36 Onsager, L., J. Am. Chem. Soc. **58,** 1486 (1936).

Op28 Oppenheimer, J. R., Phys. Rev. **13,** 66 (1928).

Pa30 Pauling, L., Phys. Rev. **36,** 430 (1930).

Pa62 Palevsky, H., J. Phys. Soc. (Japan) **17,** 367 (1962).

Pf69 Pfister, G., Ph.D. thesis, ETH, Zurich, 1969 (unpublished).

PHP69 Peressini, P. P., J. P. Harrison, and R. O. Pohl, Phys. Rev. **180,** 926 (1969).

PHP69a ——, J. P. Harrison, and R. O. Pohl, Phys. Rev. **182,** 939 (1969).

Pi49 Pirenne, J., Helv. Phys. Acta **22,** 479 (1949).

PK65 Patterson, D. A., and M. N. Kabler, Helv. Phys. Acta **4,** 75 (1965).

PN68 Pompi, R. L., and V. Narayanamurti, Solid State Commun. **6,** 645 (1968).

Po62 Pohl, R. O., Phys. Rev. Letters **8,** 481 (1962).

Po63 ——, Z. Physik **176,** 358 (1963).

Po65 Pomerantz, M., Proc. IEEE **53,** 1438 (1965).

Po68 Pohl, R. O., in *Localized Excitations in Solids*, R. F. Wallis, Ed. (Plenum Press, Inc., New York, 1968), p. 434.

Po69 ——, in *Elementary Excitations in Solids*, G. F. Nardelli, Ed. (Plenum Press, Inc., New York, 1969), p. 259.

PPHN70 Pompi, R. L., P. P. Peressini, J. P. Harrison, and V. Narayanamurti, (to be published).

Pr56 Price, P. J., Phys. Rev. **104,** 1223 (1956).

PS60 Pontinen, R. E., and T. M. Sanders, Jr., Phys. Rev. **152,** 850 (1960).

PTG69 Pohl, R. O., V. L. Taylor, and W. M. Goubanu, Phys. Rev. **178,** 1431 (1969).

PZG66 Pirc, R., B. Zeks, and P. Gosar, J. Phys. Chem. Solids **27,** 1219 (1966).

QD67 Quigley, R. J., and T. P. Das, Solid State Commun. **5,** 487 (1967); Phys. Rev. **164,** 1185 (1967); **177,** 1340 (1969).

RCK69 Rosenbaum, R. L., C. K. Chau, and M. V. Klein Phys. Rev. **186,** 852 (1969).

RF64 Reuszer, J. H., and P. Fisher, Phys. Rev. **135,** A1125 (1964).

RM59 Robinson, G. W., and M. McCarty, Jr., J. Chem. Phys. **30,** 999 (1959).

RM62 Reddington, R. L., and D. E. Milligan, J. Chem. Phys. **37,** 2162 (1962).

Ro58 Rolfe, J., Phys. Rev. Letters **1,** 56 (1958).

Ro60 Roth, L., Phys. Rev. **118,** 1534 (1960).

Ro63 Robinson, D. W., J. Chem. Phys. **39,** 3430 (1963).

Ro68 Rosenbaum, R. L., Ph.D. thesis, University of Illinois, 1968 (unpublished).

Ro69 Rollefson, R. J. (private communication).

RP69 ——, and R. O. Pohl, Bull. Am. Phys. Soc. **14,** 348 (1969).

RS61 Richards, R. E., and T. Schaefer, Trans. Faraday Soc. **57,** 21 (1961).

RTH60 Rush, J. J., T. I. Taylor, and W. W. Havens, Jr., Phys. Rev. Letters **5,** 507 (1960).

Sa66 Sauer, P., Z. Physik **194,** 360 (1966).

SBS52 Stephenson, C. C., R. W. Blue, and J. W. Stout, J. Chem. Phys. **20,** 1046 (1952).

SBS55 ——, D. R. Bentz, and D. A. Stevenson, J. Am. Chem. Soc. **77,** 2161 (1955).

Sc69 Scott, R. S., Ph.D. thesis, University of Illinois, 1969 (unpublished).

Se65 Seward, W. D., *Low Temperature Physics-LT9*, W. Daunt *et al.*, Eds. (Plenum Press, Inc., New York, 1965), p. 1130.

SE66 Schearer, L. D., and T. L. Estle, Solid State Commun. **4,** 639 (1966).

Se69 Seward, W. D. (unpublished data).

SF65 Shepherd, I. W., and G. Feher, Phys. Rev. Letters **15,** 194 (1965).

SF69 Scott, R. S., and W. H. Flygare, Phys. Rev. **182,** 445 (1969).

SH62 Savitsky, G. B., and D. F. Hornig, J. Chem. Phys. **36,** 2634 (1962).

Sh66 Shiren, N. S., Phys. Rev. Letters **17,** 958 (1966).

Sh66a Shore, H. B., Phys. Rev. Letters **17,** 1142 (1966).

Sh66b ——, Phys. Rev. **151,** 570 (1966).

Sh67 Shepherd, I. W., J. Phys. Chem. Solids **28,** 2027 (1967).

Sh69 Share, S., Ph.D. thesis, Cornell University, Cornell Materials Science Center Report No. 1158, 1969 (unpublished).

Si49 Siegel, L. A., J. Chem. Phys. **17,** 1146 (1949).

Si65 Silsbee, R. H., Phys. Rev. **138,** A180 (1965).

Si67 ——, J. Phys. Chem. Solids **28,** 2525 (1967).

Si69 —— (private communication).

SJ62 Scott, P. L., and C. D. Jeffries, Phys. Rev. **127,** 32 (1962).

SLC52 Stephenson, C. C., L. A. Landers, and A. G. Cole, J. Chem. Phys. **20,** 1044 (1952).

Sm36 Smyth, C. P., Chem. Rev. **19,** 329 (1936).

SM65 Sack, H. S., and M. C. Moriarty, Solid State Commun. **3,** 93 (1965).

Sm69 Smoluchowski, R., Proc. Colloq. AMPÈRE **15,** 120 (1969).

SMKW62 Schoen, L. J., D. E. Mann, C. Knowles, and D. White, J. Chem. Phys. **37,** 1146 (1962).

SMR30 Simon, F., K. Mendelsohn, and M. Ruhemann, Naturwiss. **18,** 34 (1930).

SN66 Seward, W. D., and V. Narayanamurti, Phys. Rev. **148,** 463 (1966).

Sp57 Sproull, R. L. (unpublished data, 1957).

SRS55 Stephenson, C. C., D. W. Rice, and W. H. Stockmayer, J. Chem. Phys. **23,** 1960 (1965).

SS69 Share, S., and H. S. Sack, Bull. Am. Phys. Soc. **14,** 346 (1969).

SSS65 Sauer, P., O. Schirmer, and J. Schneider, Phys. Status Solidi **16,** 79 (1965).

St30 Stern, T. E., Proc. Roy. Soc. (London) **A130,** 551 (1930).

ST61 Staveley, L. A. K., J. Phys. Chem. Solids **18,** 46 (1961).

St67 Sturge, M. D., in *Solid State Physics*, F. Seitz and D. Turnbull, Eds. (Academic Press Inc., New York, 1967), Vol. 20.

Su64 Sussmann, J. A., Physik Kondensierten Materie **2,** 146 (1964).

Ta51 *Tables Relating to the Mathieu Functions* (Columbia University Press, New York, 1951), p. 44.

Ta68 Taylor, V. L., M.S. thesis, Cornell University, Cornell Materials Science Center Report No. 1005, 1968 (unpublished).

Th65 Thacher, P. D., Ph.D. thesis, Cornell University, Cornell Materials Science Center Report No. 369, 1965 (unpublished; Phys. Rev. **156,** 975 (1967).

Tr49 Treloar, L. R. G., *Physics of Rubber Elasticity* (Clarendon Press, Oxford, England, 1949), Chap. II.

TS55 Townes, C. H., and A. L. Schawlow, *Microwave Spectroscopy* (McGraw-Hill Book Co., New York, 1955).

VDVR64 Venkataraman, G., V. Deniz, P. R. Vijayaraghavan, and A. P. Roy, Solid State Commun. **2,** 17 (1964).

VH61 Vedder, W., and D. F. Hornig, J. Chem. Phys. **35,** 1560 (1961).

Vr67 Vredevoe, L. A., Phys. Rev. **153,** 312 (1967).

Wa67 Walton, D., Phys. Rev. Letters **19,** 305 (1967), and in *Localized Excitations in Solids*, R. F. Wallis, Ed. (Plenum Press, Inc., New York, 1968), p. 395.

WF63 Wilson, D. K., and L. Feher, Phys. Rev. **131,** 1976 (1963).

WH50 Wagner, E. L., and D. F. Hornig, J. Chem. Phys. **18,** 296, 305 (1950).

WHDS67 Wilson, W. D., R. D. Hatcher, G. J. Dienes, and R. Smoluchowski, Phys. Rev. **161,** 888 (1967).

WK69 Wedding, B., and M. V. Klein, Phys. Rev. **177,** 1274 (1969).

WMH66 Wielinga, R. F., A. R. Miedema, and W. T. Huiskamp, Physica **32,** 1568 (1966).

WW35 Wartenberg, H. V., and G. Wehner, Z. Electrochem. Angew. Phys. Chem. **41,** 448 (1935).

YO63 Yip, S., and R. K. Osborn, Phys. Rev. **130,** 1860 (1963).

Ze65 Zernik, W., Phys. Rev. **139,** A1010 (1965).

Zi41 Ziegler, W. T., J. Am. Chem. Soc. **63,** 2700 (1941).